Department of Civil, Structural and Environmental Engineering, Trinity College Dublin

Trinity College Dublin
Coláiste na Tríonóide, Baile Átha Cliath
The University of Dublin

Design of Offshore Wind Energy Gravity Based Foundations

by

Kenneth Russell

Student #10264658

Supervisor: Prof. David Igoe

A project submitted to the University of Dublin as part of the Masters in Industry (MAI) programme

October 2020

Table of Contents

List of Figures

List of Tables

Abstract

The offshore wind is set for substantial growth globally in the coming decades. The use of Gravity-based foundations (GBF), although only 3.3% of the current installed fleet is due increase to 8.4% in the coming years. To meet this increased demand, there is a need to examine all areas of design to see where efficiencies can be achieved.

The central question to this thesis is to explore if efficiencies can be achieved in the design of gravity-based foundation (GBF) for offshore wind turbines and if a reduction in quantity of material required to ballast the structure is possible. It does this through setting out an alternative approach to calculation the roughness parameter (r), applying this in lab experiments, carrying out a worked example to quantify ballast material savings and carrying out stability checks on the GBF in a 3DFE analysis.

The refined approach used was to apply the definition of the roughness coefficient (r) for cohesionless soils was to the problem i.e. the tan of the interface friction angle (tan δ) divided by the tan of the soils internal friction angle (tan ϕ'). Lab testing was carried to out to obtain tan δ and tan ϕ' for a range of soil types and interpret an (r) value a smooth and serrated based bottom.

An analysis was carried out to compare the pre-2014 DNV method of calculation (r) to the suggested refined approach and quantifies potential ballast material savings. The results showed how a 29% saving in ballast can be achieved; the minimum required ballast weight using this approach is reduced from 26.993 kTonne to 19.081 kTonne (approx. 8 kTonne). It also provides likely savings in ballast required for a range of seabed conditions (fine grained SAND to sandy GRAVEL). It concludes sliding capacity still governs design for friction angles below 43°; above this value overturning is the governing factor and no ballast savings can be achieved.

A 3D finite element stability analysis was carried out on the GBF in Plaxis 3D. Analysis showed that with increased loading the vertical displacement increases; a 20kTonne results in a 50mm, 30kTonne equating to 92mm and 40kTonne results in a 104mm within the permitted FoS, thus proving that the bearing capacity is sufficient in Blessington Sand to support the fully ballasted GBF. Tilt was examined and findings showed that only the differential settlement associated with the 20kTonne ballasted GBF (ΔS = 185 mm) was within the tilt tolerance of 0.25°. Ballast weights of 30kTonnes and above would require seabed preparation i.e. installation of coarse material between GBF and the seabed.

The main contributions this thesis offers offshore designers are steps to applying an alternative approach to estimating sliding resistance, and quantifies the amount of ballast that can be saved by using this approach.

Declaration

Aside from carrying out the testing of the commissioned laboratory work in Section 4, I hereby declare that this is entirely my own work and that it has not been submitted as an exercise for the award of a degree ar any other university. I agree to deposit this thesis in the University's open access institutional repository or allow the library to do so on my behalf, subject to Irish Copyright Legislation and Trinity College Library conditions of use and acknowledgement

Nomenclature

Abbreviations

API	American Petroleum Institute
BS	British Standard
CIRIA	Construction Industry Research and Information Association
DNV- GL	Det Norske Veritas-Germanischer Lloyd
EC	Eurocodes
FEA	Finite Element Analysis
FEM	Finite Element Method
FoS	Factor of Safety
FoS Utilisation	FoS/minimum FoS required
GBF	Gravity Based Foundation
GDG	Gavin and Doherty Geosolutions Ltd
HLV	Heavy Lifting Vessels
HS	Hardening Soil (HS) model
HSSmall	Hardening Soil model with small strain stiffness
ISO	International Organization for Standards
O&G	Oil and Gas
PSD	Particle Size Distribution
RNA	Rotor Nacelle Assembly
SEAI	Sustainable Energy Authority of Ireland
SLS	Serviceability limit state
SF	Safety Analysis
UDL	Uniformly Distributed Load
ULS	Ultimate Limit State

Latin Symbols

A_{eff}	Effective area
B	Width of the footing
c	Design cohesion or design undrained shear strength (kN/m2)
c'	Effective cohesion of the soil
d_y, d_q, d_c	Correction factors depending on the depth of the foundation
D_{50}	Mean particle size
D_r	Relative Density
E'	Young's Modulus
E_{50}^{ref}	Triaxial loading stiffness
E_{oed}^{ref}	Odeometer loading stiffness
E_{ur}^{ref}	Triaxial unloaded stiffness
F_y	Horizontal loading (Plaxis)
F_z	Vertical loading (Plaxis)
G	Gravity
G_0^{ref}	Strain shear modulus
H	Horizontal loading
H_{max}	Horizontal resultant force at the base.
i_y, i_q, i_c:	Correction factors depending on the shape of the footing
M_{res}	Resistant moment
m	Rate of stress dependency
M_x	Moment (Plaxis)
N_c, N_q, N_y	Bearing capacity factors (depending on the friction angle)
q	Overburden pressure at the level of the foundation-soil interface (kN/m2)

q_d	Design bearing capacity (kN/m2)
r	Roughness parameter/coefficient
R_a	Ratio of surface roughness
R_{inter}	Strength reduction factor in Plaxis
R_k	Characteristic resistance
S_k	Characteristic load/moment
S_y, S_q, S_c	Correction factors depending on the shape of the footing
U	Total displacement (Plaxis)
U_y	Lateral displacement (Plaxis)
U_z	Vertical displacement (Plaxis)
V_{ur}	Poisson's ratio
V	Vertical load acting during the relevant loading condition

Greek Symbols

Υ	Unit weight of soil (kN/m3)
Υ_{sat}	Effective submerged unit weight
$\gamma_{0.7}$	Strain level where shear modulus is reduced to about 70% of small-strain shear modulus
ΔS	Differential settlement (mm)
φ	Internal friction angle of soil
φ'	Effective internal friction angle of soil
δ	Interface friction angle (between the foundation soil and the structure)
(φ_{cv})	Constant volume friction angle
∑Msf	Global factor of safety in Plaxis
ψ	Peak friction angle

Acknowledgements

This thesis was initially conceptualised by my employer, Gavin & Doherty Geosolutions Ltd. and is based on a project I worked on for the SEAI. Thanks to Prof. David Igoe who acted as my supervisor for this project and offered invaluable advice and insight all through the research. I would like to thank the Head of Offshore in GDG, Dr. Soroosh Jalilvand for his support. I would sincerely like to thank my Fiancée, Michelle, for her patience and for looking after our boys, Jonah and Julien while I worked in this thesis.

1 Introduction

This thesis comprises of eight chapters. The material presented in each chapter covers a specific part of the research conducted. The sections combined offer opportunity for the enhancement of sliding capacity for offshore wind turbine on various seabed types during early stage design. Figure 1-1 illustrates the structure of this thesis.

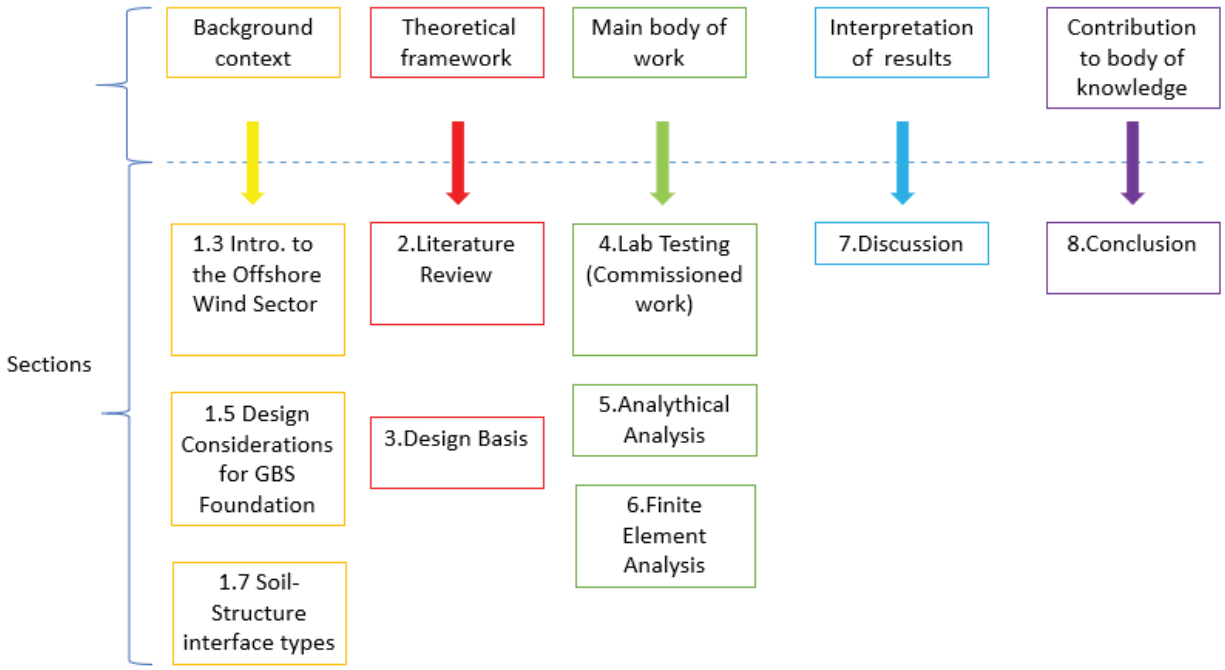

Figure 1-1: Thesis structure

1.1 Methodology and Thesis Sections

Section 1.2 and Section 1.3 provides a background to the research and the offshore wind industry. Section 1.4 provides a context of GBFs in the offshore wind sector. Design considerations GBFs are outlined in Section 1.5.Installed GBFs, suitable seabed types and a range of soil-structure interface options are presented in sections 1.6 and 1.7.

A literature review is provided in Section 2.1 outlines how sliding resistance have been calculated using Det Norske Veritas-Germanischer Lloyd (DNV-GL) standards and suggests an alternative approach based on work carried out to help decode the Eurocode 7 (Bond & Harris, 2009). A critical analysis of some similar studies into the behaviour soil-structure interaction of GBFs is put forward in Section 2.2. The development of FEM in geotechnical engineering and its importance in studying the behaviour of GBF are outlined in Section 2.3. Finally, the research objectives are stated at the end of the literature review.

Section 3 sets out the design basis of this thesis and all relevant calculations, formulae and assumptions for the calculations and inputs to the finite element analysis (FEA) components of this MAI project. The geometry of the GBF, water depth and hydrodynamic loads were adopted from ARUP's GBF (Smith, et al., 2015) and the turbine interface loads were selected based on reference loads for a 10MW DTU offshore wind turbine (Velarde, 2016).

The laboratory testing phase (Section 4) of this industry-based MAI project was commissioned by Gavin and Doherty Geosolutions Ltd (GDG) as part of work carried out on behalf of the Sustainable Energy Authority of Ireland (SEAI), the testing took place in Trinity College Dublin (TCD). The addition of Blessington sand as a soil grading was carried out at the request of the author of this thesis. A series of interface shear tests were undertaken to demonstrate improved sliding resistance for a range of soil gradings and structural interfaces i) smooth pre-cast concrete, and ii) a ridged concrete interface. Data from there tests were interpreted and a range of values for the interface friction angle, sliding ratio and roughness parameter (*r*) were derived and used in the ballast requirements (Section 5) and FEA (Section 6).

Section 5 demonstrates saving (in the form of a reduction in the quantity of ballast material required) that can be achieved from the adoption of the refined approach (improvement on the DNV pre 2014 method) for calculation of sliding resistance, bearing capacity and overturning through a preliminary design example for a gravity base foundation supporting an offshore wind turbine in 45 m water depth through a series of hand calculations.

The Finite Element Analysis (FEA) software Plaxis 3D is employed in Section 6 to analyse the behaviour of the GBF outlined in Section 3.2 when a series of potential ballast loads are applied. The FEA quantified vertical and lateral displacements for a serrated base within a factor of safety. The differential settlement is also calculated.

A discussion on the meaning on the results is presented in 7. The significance of the findings is highlighted and its applicability to industry is underlined. Some limitations of the thesis are mentioned and the potential for further study suggested.

Throughout the thesis numerous values and calculation are used. The source, formulae and calculations are presented the literature review and design basis and then applied in the main body of the thesis i.e. Sections 4, 5 and 6. Table 3-10 outlines the relationship of values and calculations used.

1.2 Background to the Research

Key factors in the design of GBF are the estimation of sliding capacity, bearing capacity and overturning. The sliding capacity in conventional concrete GBF concepts is provided by interface friction at the base of the foundation, as well as, secondary mechanisms such as particle interlock and passive resistance due to shallow penetration of the foundation in the seabed. In areas with coarse seabed or shallow bedrock, where limited penetration is available and skirts are not feasible, the sliding capacity of conventional concrete GBF is mainly governed by the interface friction at the base. Current design guidelines provide recommendations for assessing the friction resistance as a function of the dead weight of the structure. However, these approaches are limited in range of interface geometries considered and tend to underestimate the friction. These standards also provide limited insight into the sliding resistance for uneven seabed with coarse surface material such as gravel, boulders and cobbles.

Despite the limited commercial application within the offshore renewable industry to date, GBFs have advantages over steel piled foundations with respect to;

- Fatigue life;
- Environmental impact through installation noise;
- The need for less specialist fabrication facilities
- Straightforward deployment strategy that is well suited to the narrow weather windows associated with offshore construction, and in specific.

Presently there are certain combinations of ground conditions and structure type where the use of a GBF is often considered not feasible as the size of the structure required to resist the lateral and moment loading is too large. Examples of such situations include;

- Areas with shallow bedrock underlying sandy seabed, which may limit the possibility of adoption of skirts to the required embedment depth;
- Areas with coarse seabed where there is a mix of gravel, boulders and or a hard and uneven surface, where seabed preparations required to achieve a flat seabed would be too costly.

The traditional estimation of this friction resistance in areas with coarse seabed materials is directly proportional to the dead weight of the substructure. Therefore, to increase the sliding capacity of the substructure, it is necessary to increase its dead weight using additional ballast or material weight. This can be very costly due to requirement for procurement, staging and

installation of additional ballast, as well as potential increase in the overall size of the structure that will subsequently increase the requirements for installation vessels. Additionally, the larger structure will attract higher hydrodynamic loading, which in turn, will increase the demand for additional ballast or larger footprint of the structure.

To address this issue, and aid in the further development of GBF for marine renewables, this MAI project aims to further the knowledge of design by refining the design approach and prove that a reduction in the quantity of ballast material required can be achieved.

1.3 Introduction to Sub-Structures in the Offshore Wind Sector

Figure 1-2 shows the current worldwide mix of substructure types for projects operating at the end of 2018 along with the projected substructure types for the 37,203 MW of proposed that have announced their intended substructure. In 2018, monopiles continued to dominate the operating fleet of global offshore wind turbines, representing 73.5% of the total market. According to The US Dept. of Energy (2018) alternative substructure types, such as gravity-base (3.3%), jacket (6.5%) and tripod (4.7%) represent a much smaller share. High rise pile caps are included in this figure, whereas they are absent in the European market.

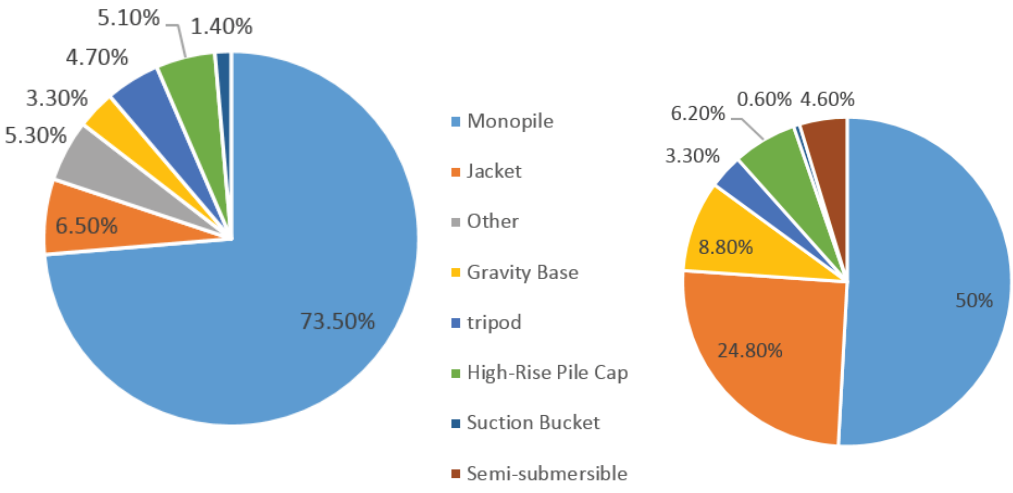

Figure 1-2: Worldwide trend in foundation type – comparison between commissioned installations up to the end of 2018 (left) and (right) future projects that have disclosed their foundation type (DOE, U.S, 2018)

Looking at future projections, on the right side of Figure 1-2, developers have indicated they plan to increase the use of jackets fourfold (increasing to 24%). This change corresponds to projects being developed in deeper water depths and with larger turbines. Gravity-base foundations will

also slowly increase their market penetration (increasing to 8.8%). This is anticipated to be because they do not require pile driving during installation, hence eliminating underwater noise and associated negative impacts to marine mammals. Floating foundations are required for projects in water deeper than 60 m and will become more common, projected to increase to 4.6% of total (DOE, U.S, 2018) in the coming decade.

In Europe, monopiles remain the most common substructure type. According to Wind Europe's key trends and statistics of offshore wind (WindEurope, 2019) the total installed fleet, monopiles represents 81.5% (4105 turbines) of all installed substructures, Jackets 8% (403 turbines) and GBF 6 % (301 turbines). Figure 1-3 shows turbine foundation type used in European offshore wind projects and (on the right) a schematic of typical foundation types.

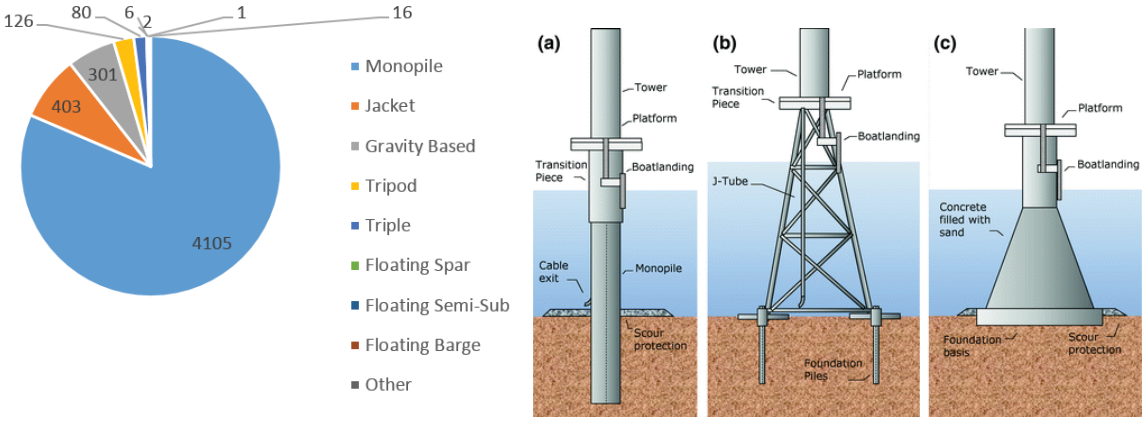

Figure 1-3: Turbine foundation type used in European offshore wind projects (left) (WindEurope, 2019) and on the right schematic of typical foundation types (Klijnstra, et al., 2017)

Figure 1-4 shows the CAPEX baseline for a typical offshore wind farm. Foundations and foundation installation combined account for 24% of the overall cost.

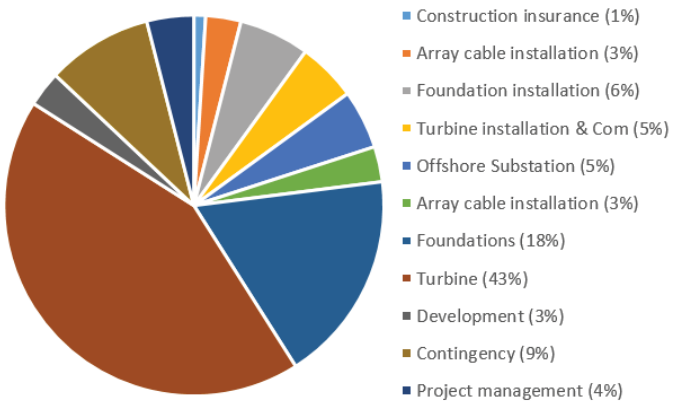

Figure 1-4: CAPEX baseline for a typical offshore wind farm, €, kW (WindEurope, 2019)

Offshore wind energy output capacity has grown year on year over the past 2 decades (from under 1 GW cumulative capacity in 2000) to circa 20 GW in 2018 and is predicted to grow to 520 GW by 2050 (Figure 1-5). Recent data and research findings confirm the rapid capacity growth, ongoing cost and performance improvements, increasing technological sophistication and continued need for international standardisation for new technologies. From 2020 to 2022 the cost of electricity from newly commissioned offshore wind power projects will range from USD 0.06/kilowatt-hour (kWh) to USD 0.10/kWh based on current trends (WindEurope, 2019).

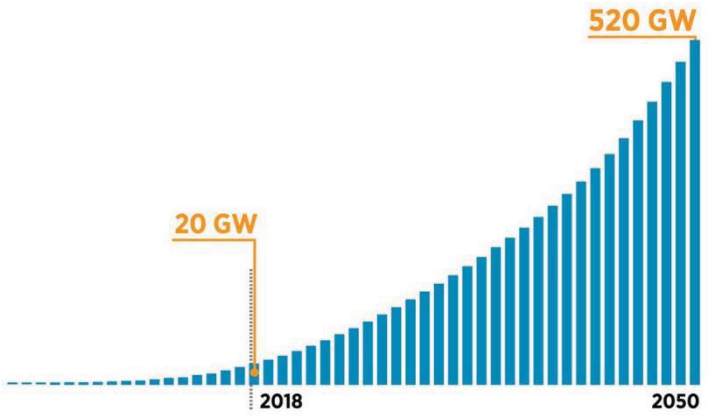

Figure 1-5: Historical and projected cumulative installed capacity of offshore wind, 2000-2050 (WindEurope, 2019)

Offshore wind is growing steadily but still faces challenges including deployment related to resource characterization, grid interconnection and infrastructure barriers. The goal is now in optimisation of materials, construction technology, transportation/installation and, also, vessel spread etc.

1.4 The Use of Gravity Based Foundations for Offshore Wind Turbines

With the number of offshore wind farms rapidly increasing and in a wide variety of site conditions and using different turbine sizes, the need for alternative support structures other than the

conventional monopile structure is apparent and several projects have been realised using other support structure types (De vries, 2011).

GBFs are flat-based-bottom support structures utilizing their self-weight to withstand overturning moment and sliding shear and held in place by gravity. They are normally constructed with reinforced concrete and vary in geometry, size and weight depending on specific design cases. Most recent GBFs have been constructed as hollow concrete shells for ease of transport and installation. The design will include a central shaft (steel or concrete) for transition to the wind tower. Once in position the structure is ballasted with concrete, sand, rock, iron-ore and/or other material to increase the supporting weight. Larger GBFs have been used traditionally in deeper waters by the O&G industry, there is scope for technology transfer to the offshore renewables.

According to Wind Europe (2019) GBFs have mostly been used on northern European offshore wind projects (203 turbine installations up to 2015) in shallow waters (<25m). To date, ground condition conducive to GBFs include shallow bedrock, rock, course gravel, dense sand and highly over consolidated clay. Also, in challenging geology where it would be difficult to install piles.

The principal phases according to Esteban et al. (2015) of offshore wind projects are seabed preparation, support structure manufacturing, support structure transport, support structure installation, ballasting and anti-scour protection, O&M and decommissioning

There are advantages to choosing a gravity-based foundation solution ahead other foundation option. Most importantly, piling is not required. Structures are generally made from durable reinforced concrete and low maintenance with most of the structure above seabed level, repositioning is also possible. However, seabed preparation (e.g. dredging, installation of course material etc.) is required and transportation costs are high with the need for heavy lifting vessels (HLV). GBFs require a competent homogenous seabed e.g. dense sand, stiff clay or shallow bedrock, in less competent soil types GBFs would be susceptible to large settlement and bearing capacity concerns due to the very large weight of the ballast. Using concrete as the principle material makes the project less dependent the fluctuating price of steel (Attari, et al., 2014) the foundation costs (incl. installation) accounts for almost a quarter of the overall.

Furthermore, concrete requires a lower maintenance and has a long-lasting life cycle within the marine environment. Moreover, gravity-based structures avoid tensile loads between the bottom of the foundation and the soil. This is accomplished by keeping the stability of the structure through sufficient quantities of loads. Whether there are relatively low loads or ballast, which are

easily and cost efficiently provided, GBFs are considered a highly competitive foundation (4COffshore, 2018).

Disadvantages associated with the installation of GBFs include the need for seabed preparation (not required with other types of support structures such as monopiles and jackets). Their weight (1,900 to 4500 tonnes) with additional large volumes of ballast required (15- 40kTonne installed on site) requires a quay with high bearing capacity. The water depths where they can operate are limited. Liquefaction of the soil beneath the base due to cyclic loading must be addressed when assessing the stability of the foundation (De vries, 2011). Table 1-1 gives a summary of the advantages and disadvantages on GBFs.

Table 1-1: Summary of advantages and disadvantages of GBFs

Advantages	Disadvantages
No piling operations required, this can be a significant advantage where there is shallow bedrock and/or there are environmental (noise) constraints;	Seabed preparation is necessary before deployment of the structure;
The next generation is projected to be self-Buoyant structures which will permit a "float-out" to site installation;	A very heavy structure (1,900 to 4500 tonnes) with additional large volumes of ballast required (15-40kTonne installed on site). This requires a quay with high bearing capacity;
Concrete is readily available and economical compared to the steel;	Large space is required at quayside required, for future projects each GBF will have a base diameter of 30-40m, and may will have to be fabricated and stored prior to installation;
Low maintenance needed as concrete is inherently durable in marine environments.	Unsuitable for sites with soft soils, or undulating rocky sea beds.

The first use of GBFs in the offshore wind sector was at Vineby, Denmark in 1991. It was installed at a water depth of 4m and 2km from the shoreline. It supported a 450 KW turbine with rotor diameter of 35m and hub height of 35m before being decommissioned in 2016. Between 1991 and 2015 the use of GBFs increased in the North Sea area with installations off the coast of Denmark. (e.g. Tunø knob), Germany (e.g. Breitling), Sweden (e.g. Kårehamn), Belgium (e.g. Thornton Bank Phase 1 – depth 27.5m) and France (e.g. Fecamp – floating GBF). Table 1-2 provides a table of operating offshore wind farms GBF installed to date.

Table 1-2: Records of operating GBF foundations in offshore wind farms (Attari, et al., 2014)

Offshore Wind Farm	Country	Turbine Capacity (MW)	Installed Capacity (MW)	Number of turbines	Water depth (m)	Distance from shore (km)
Avedore Holme	Denmark	3.6	10.8	3	0.5 to 2	0.05 to 0.1
Breitling Demonstration	Germany	2.5	2.5	1	2	0.5
Choshi Offshore Demonstration Project	Japan	2.4	2.4	1	12	3.1
Ems Emden	Germany	4.5	4.5	1	3	0.5
Kemi Ajos	Finland	3	30	10	3 to 8	2.6
Kitakyushu Demonstration	Japan	2	2.0	1	14	1.4
Kårehamn	Sweden	3	48	16	8 to 21	7
Lillgrund	Sweden	2.3	110.4	48	4 to 10	7
Middelgrunden	Denmark	2	40	20	3 to 5	2
Nysted 1	Denmark	2.3	165.6	72	6 to 10	10.8
Pori Offshore 1	Finland	2.3	2.3	1	9	1.2
Rodsand 2	Denmark	2.3	207	90	6 to 12	8.8
Rønland	Denmark	2.15	17.2	8	0 to 2	0.1
Sprogø	Denmark	3	21	7	6 to 16	10.6
Thornton Bank 1	Belgium	5	30	6	12 to 27.5	26 to 27
Tunø Knob	Denmark	0.5	5	10	3 to 6	6
Vindeby (Decommissioned 2015)	Denmark	0.45	4.95	11	2 to 6	1.5 to 3
Vindpark Vanern	Sweden	3	30	10	3 to 13	7

1.5 Design Considerations

Existing offshore design codes have their origins in the O&G industry and have been adapted by the offshore renewables industry. O&G platforms have more stringent safety requirements and therefore have been traditionally designed with safety in mind, whereas offshore wind turbines

are unmanned structures where the consequences of failure are significantly lower, and therefore do not need the same amount of conservatism. Figure 1-6 compares typical foundation loading values for and O&G platform and >10 MW turbine (with a monopile foundation in this example).

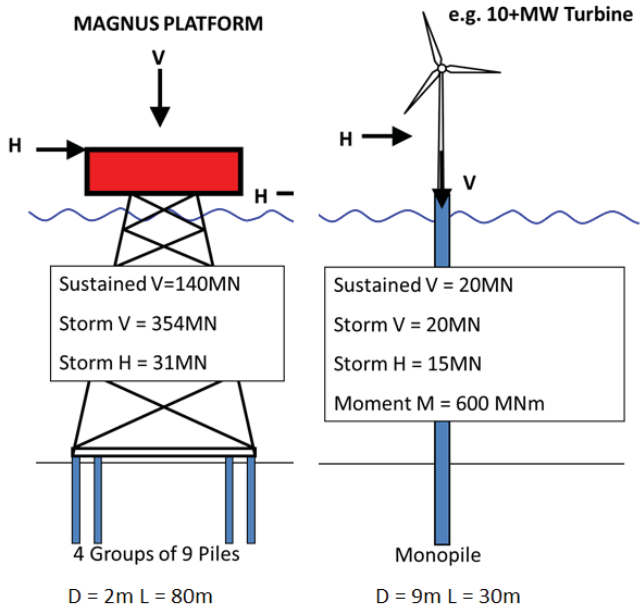

Figure 1-6: Typical foundation loading for (a) an O&G platform and (b) a monopile supporting a 10MW OWT (Igoe, 2018)

By justifying higher friction values, gravity substructures can become more efficient and require less material, which in turn will require a smaller vessel spread and reduced CAPEX.

Aside from the overall stability of the structure under moment equilibrium, the main geotechnical considerations for Ultimate Limit State (ULS) relate to the bearing capacity of the soil beneath the foundation and its resistance to sliding. Figure 1-7 shows some of the ULS failure mechanisms which should be considered for GBF design. The foundation should be designed to be sufficiently robust so as to prevent failure from any of these mechanisms. Bearing capacity failure is usually prevented by ensuring that the foundation diameter (or breadth) is sufficiently large so that the pressures exerted by the structure are smaller than the bearing capacity of the soil. Sliding is usually prevented by ensuring the GBF has enough weight or ballast to develop sufficient friction at the base of the foundation. These two criteria often work against each other, i.e. increasing the weight (or ballast) will increase the margin of safety for the sliding verification but reduce the margin of safety for the bearing capacity verification. Optimising the costs of GBF is therefore often a trade-off between reducing ballast weight and increasing the base diameter (or vice-versa).

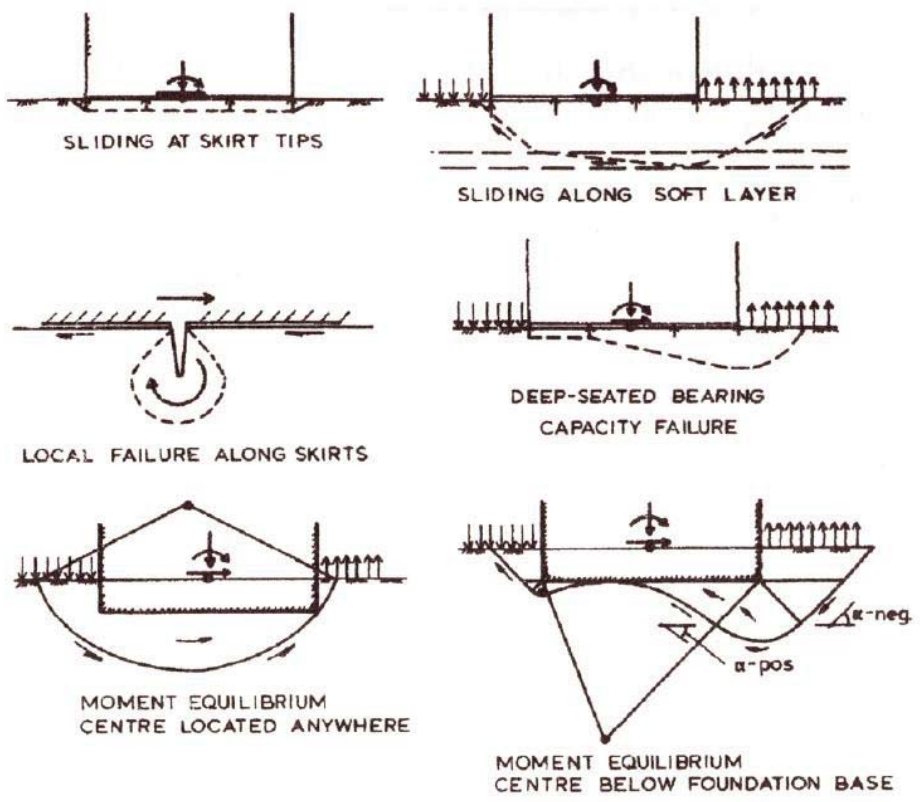

Figure 1-7: Examples of possible failure mechanism of GBFs after (DNV-GL, 2017)

While a large amount of experience on the design of GBFs has been developed by the O&G industry, the design requirements for offshore renewables are often quite different. An O&G platform often has a very heavy topside and the vertical loads are typically an order of magnitude more than the horizontal loads coming from wind and wave action. A wind turbine, on the other hand, is a comparatively light structure and the horizontal loads are of similar magnitude to the self-weight of the structure. The much lower vertical loading from OWTs supported on GBFs mean that sliding can often be a governing design criterion (see Figure 1-6).

Compared to the slender monopile the GBF had much higher hydrodynamic forces to resist. The shape of the foundation is important and has a bearing on the structure's ability to withstand hydrodynamic loading, susceptibility to overturning and scouring.

Scour protection is an essential part of design and generally involves the post installation placement of material around the foundation. Seabed interface option include skirting, saw tooth and shear key. Design to mitigate against ice loading is also required in colder regions.

The design codes also address this aspect of offshore engineering; DNV-GL-RP-212 (DNV-GL, 2017) states that "the interaction between a structure and the soil through the structural

foundation elements, such as the baseplate and skirt of a GBFs has an influence on several aspects of structural response namely:

- Global response of dynamically sensitive structures where the foundation stiffness may strongly influence the response;
- Contact stresses between soil and structural elements, governed by soil stiffness and strength and by structural stiffness;
- Settlements of a GBFs;
- Stresses in and displacement of piles and structural elements of a jacket platform, governed by the soil strength and by the stiffness of the piles and structure (DNV-GL, 2017).

1.6 Installed Gravity Based Foundations – Design and Seabed Characteristics

In challenging geology where it would be difficult to install piled GBFs have also been considered. All Danish projects (see Table 1-2) were installed in shallow rock and clay, Lillgrund and Kårehamn in are also in shallow rock and clay while, Thornton Bank, Phase 1 in medium grain dense sand. Geotechnical and geophysical investigations identify potential areas and generally material with low bearing capacity are dredged e.g. loose sands, muds, clays and silt; thickness of the layers to be removed can be as deep as 10m (de Temiño, 2013). Installed GBFs have been used where seabed conditions were coarse to medium dense sand with a gravelly horizon at the bottom and predominantly chalk.

The geometry of the GBF system is an essential consideration of the design process, with each design carefully considered to meet the need of each specific site. This has evolved from earlier projects to facilitate installation in deeper waters, Figure 1-8 show a basic evolution of this geometry.

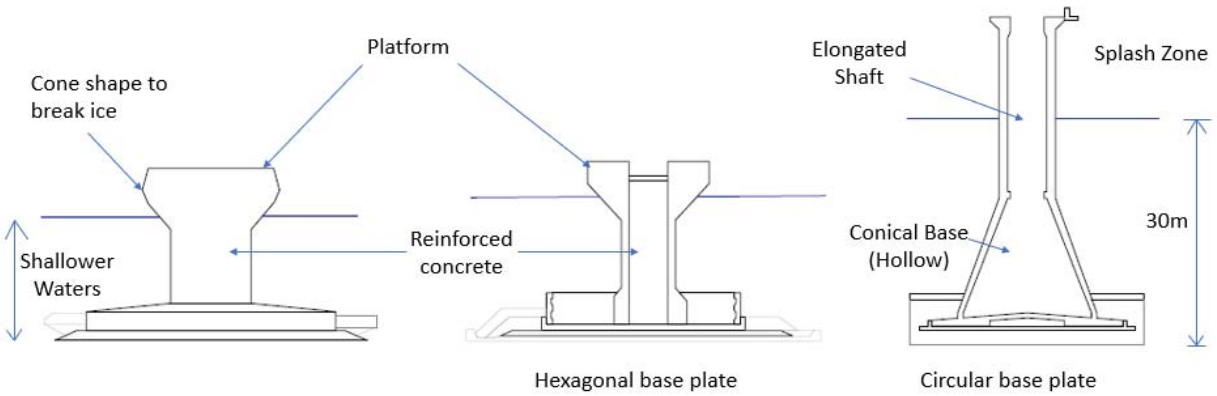

Figure 1-8: Basic schematic of the evolution of the GBF with 3rd generation on the right (Esteban, et al., 2015)

Installed offshore wind GBF footing sizes range from 17m diameter to 25m for the conical designs and an average of 17m x 17m for the rectangular designs. A number of different footing shapes have been used:

- Circular base plate with a conical section and a cylindrical section;
- Rectangular base plate with pre-stressed box;
- Rectangular base plate with penetrative concrete legs;
- Hexagonal base with concrete caisson structure;
- Elliptical with partitioned cells for ballast;
- Square based bottom.

Figure 1-9 illustrates four GBF designs that will be examined in closer detail, they are:

- Seatower “Crane-Free” Gravity Based Foundation
- The BAM Gravity Based Foundation Design
- The Strabag Gravity Based Foundation Design
- The Ramboll, Freyssinet and BMT Nigel Gee Gravity Based Foundation Design

Figure 1-9: Image of other GBFs considered. Top left: Crane-Free Gravity Base (Seatower, 2013), top right: BAM Van Oord, bottom left: Strabag & Bottom Right: Ramboll, Freyssinet/BMT Nigel Gee (The Carbon Trust, 2015)

1.6.1 Seatower "Crane-Free" Gravity Based Foundation

The first Seatower Cranefree gravity foundation for offshore wind has been successfully installed in the British Channel approximately 15 km off the French coast at the Fécamp offshore site at 30 meters water depth. The "crane-free" gravity base concept is a concrete structure with a relatively thin slab, an intermediate-length conical part, and a cylindrical shaft in the upper part. This concept was designed, with a hollow interior to be transported by floating out to site with the support of tugboats, this avoids the use of an expensive and weather-sensitive cranes (Seatower, 2013).

1.6.2 The BAM Gravity Based Foundation Design

This GBF is made up of more than 1,800m^3 of concrete and weighs over 15,000 tonnes when fully installed on the seabed with a total height of around 60 metres from the base to the access platform (BAM, 2017). It is conical shaped structure with a circular base diameter of 40m.

1.6.3 The Strabag Gravity Based Foundation Design

Both of the Strabag's GBF designs have a geometrical slab and a cylinder in the upper part and use the pre-stressed concrete technique, they are suitable for water depths up to approximately 45 m. The concepts employ a joint transportation and installation of the foundation and the wind

turbine generator which reduces the number of operations carried out at sea during the installation phase allow the structure to be completely disassembled. A purposed vessel is used, called STRABAG Carrier is used to transport and installation. A lifted design using a floated crane. Pre-stressed concrete is used and small skirts may be required depending on soil conditions. Integrated footing plates are used for load transfer from concrete to soil and to avoid gaps between concrete and soil and developing of scour (The Carbon Trust, 2015).

1.6.4 The Ramboll, Freyssinet and BMT Nigel Gee Gravity Based Foundation Design

This design uses an integrated approach to onshore construction, transportation and offshore installation. It employs a specialised semi-submersible transportation and Installation barge where the turbine and tower can be pre-installed onshore if required (The Carbon Trust, 2015).

1.7 A review of Soil-Structural Interface Types

Some installations are designed to require no penetration while others require a penetration to withstand horizontal loading and shear forces. The sliding resistance will always increase where there is significant seabed-structure penetration. This section reviews the following interface options:

- Skirting
- Concrete Grouted Interface
- Flat based bottom
- Serrated based bottoms

1.7.1 Skirting

In O&G installations seabed penetration can be achieved through the use of a “skirt” at the base of the GBF. however, no evidence was found that skirting has been used on the installations of offshore wind farms. Skirting has been employed to increase the sliding resistance, transfer loads to where the soil is stronger, provide a closed compartment to facilitate grouting under base and provide scour protection. The foundation penetrates into the seabed, increasing the bearing area. The load is transferred down to the underlying layers, lateral load capacity is improved by the skirt’s lateral resistance and the moment load capacity raised, and the foundation resists uplift better (Ahmadi & Ghazavi, 2012).

Skirting runs along the edge (and sometimes additional skirts internally) penetrating into the ground below the seabed. The penetration depth of the skirts can range from 0.5m to 30 m, depending on the softness of the underlying soil and size of the upper structure (Gourvenec & Barnett, 2011). The skirts form an enclosed space where the soil is confined and works as a unit

with the overlain foundation to transfer superstructure load to soil essentially at the level of skirt tip. Reinforced concrete skirts have also been used on concrete structures. Figure 1-10 illustrates a skirt on the flanks of a GBF.

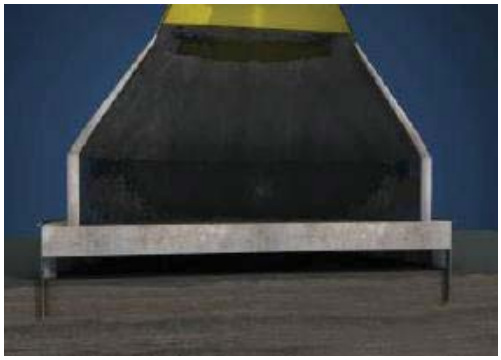

Figure 1-10: Image of a skirt on the flanks of a GBFs (Seatower, 2013)

1.7.2 Concrete Grouted Interface

Grout is used to assist with securing structures to the seabed. The use of grout in O&G GBFs is commonplace and has been used to carry out the following function:

- avoid further penetration and to keep the platform vertical;
- ensure uniform stresses against the foundation slab and avoid unintended overstressing of structural elements during continued ballasting and environmental loading;
- prevent piping from water pockets below the base during environmental loading (Tistel, et al., 2015)

In the offshore sector wind grout can be used similarly. It has been applied at Seatower's Crane-free demonstrator project where grout was pumped in between the seabed and the soffit GBF to fill the void and to provide fill contact (de Temiño, 2013).

1.7.3 Flat Based Bottom

Some GBF installations proceed without any penetration into the sea bed e.g. where a flat bases bottom is used. This seems to have been the case in offshore wind to date. This is backed up by Temiño's master's thesis (2013) statement that "skirting has not yet been introduced into offshore wind it was assumed that all of the installations to date are flat based bottomed". Figure 1-11 shows an example of a flat-based-bottom GBF.

Figure 1-11: Thornton Bank, Phase I - flat based bottom GBF at quayside (Piere, 2009)

1.7.4 Serrated Based Bottoms

Greater soil-structure contact can be achieved by employing a serrated (or grooved base). This system was used in the Demogravi3 research project in Portugal and the met meteorological Mast from Moray Firth Offshore Wind Farm, Scotland. Figure 1-12 illustrated the general design of the groves at the base of a serrated based bottom.

Figure 1-12:Example of a serrated based bottom design

2 Literature Review

This literature review aims to provide an evaluative critique into work done in the area of offshore renewables design codes, experimental and numerical analysis of GBFs behaviours and the use to date of FEM in geotechnical engineering. The intention is to bring the reader up to date on the range of knowledge that has been established on these topics and identify any gaps; the work contained in this thesis seeks to go beyond these gaps and add to the body on knowledge in this area.

GBFs sliding resistance in current offshore design codes show a deviation between different design standards (*r*). A review of some recent studies of soil-structure (GBF) interaction - investigation sliding resistance, bearing capacities and Plaxis modelling is presented and the strengths and weaknesses of these studies are expressed by the author. The origins and importance of FEM in geotechnical engineering along with the selection of an appropriate FEM package and constitutive soil model are outlined.

By presenting this literature review a strong case is built to justify the current study.

2.1 Design Codes and Standards for Gravity-Based Structures

All offshore design and construction must adhere to strict codes and standards to maintain high safety and structural standards. These standards have been developed for the oil and gas (O&G) industry, principally by the API over the past century and were developed to meet the specific needs the sector. DNV were the first institution to adapt a set of codes for offshore wind in 1992. Offshore windfarms are typically built in relatively shallow waters <50m, in areas where suitable wind regimes are harnessed and converted into electricity, whereas oil platforms are typically installed in much deeper waters to aid extraction from oil/gas fields. Some O&G platforms are designed to be manned whereas offshore wind turbines are not. Extreme wave loads generally govern the design of conventional fixed offshore platforms with wind loads contributing a mere 10 percent to the total load. Therefore, existing offshore standards emphasize wave loading but pay little attention to the combination with wind loads (Malhotra, 2011). On the other hand, offshore wind turbine design is generally governed by extreme wind, wave and current loads.

Key standards bodies in the offshore renewables include DNV- GL, API and the International Organization for Standards (ISO). These institutions provide detailed guidelines for all aspects of offshore energy engineering from initial design to operation and maintenance to decommissioning. The main design standards relevant to geotechnical design of offshore GBFs and this study are:

- DNV-OS-J101 (2013) – Design of Offshore Wind Turbine Structures (superseded) (DNV-GL, 2013)
- DNVGL-ST-0126 (2018) – Support structures for wind turbines (current) (DNV-GL, 2018)
- DNVGL-RP-C212 (2017) – Offshore soil mechanics and geotechnical engineering (current) (DNV-GL, 2017)
- ISO-19901-4 (2014) – Petroleum and natural gas industries – Specific requirements for offshore structures – Part 4: Geotechnical and foundation design considerations (current) (ISO, 2014)
- API-RP-2GEO (2011) – Geotechnical and foundation design considerations (current) (API, 2011)

The treatment of the bearing capacity of GBF systems is broadly similar across all these standards, having been developed originally by the O&G industry (API standards). The treatment of sliding resistance for GBFs deviates somewhat between different design standards. The API-RP-2GEO (API, 2011) standards propose the maximum horizontal load for the extreme condition of pure sliding should be limited to:

$$\mathrm{H} = V.tan\,\varphi' \qquad \text{Equation 2-1}$$

Where H is the maximum total horizontal load applied to the base of the foundation at failure under drained conditions, V is the actual vertical load acting during the relevant loading condition, φ' is the soils internal friction angle. The guidelines suggest that this equation assumes that the full soil resistance in mobilised along the interface between the foundation and the soil (i.e. full soil-soil contact is assumed) which should be assessed on a case by case basis. It is also suggested that it may be more appropriate to consider the use of different interface friction angles, δ, between the foundation soil and the structure. The equation would therefore become:

$$H = V.\tan\delta \qquad \text{Equation 2-2}$$

The DNV approach for sliding varies from the API approach somewhat. Prior to 2014 DNV guidelines (DNV-GL, 2013) suggests that “foundations subject to horizontal loading must be investigated for sufficient sliding resistance”. Such foundations must meet the following criterion:

$$H < A_{eff}.c' + V.tan\varphi' \quad \text{Equation 2-3}$$

Where A_{eff} is the effective area of the foundation and c' is the effective cohesion of the soil. These guidelines also state that the ratio of horizontal friction to vertical load must be limited to 0.4, such that:

$$H/V < 0.4 \quad \text{Equation 2-4}$$

Hence, for a cohesionless soil the equation simplifies to: φ

$$H/V < \min(tan\varphi', 0.4) \quad \text{Equation 2-5}$$

More recent updates to the DNV design standards (DNV-GL, 2017), have modified the above equations by removing the maximum H/V ratio of 0.4 and using a roughness parameter (*r*). which is a factor with a value of 1.0 for soil against soil and takes lesser values for soil against structure. Hence, the updated form of calculating horizontal sliding resistance is:

$$H < r.\left(A_{eff}.c' + V.tan\varphi'\right) \quad \text{Equation 2-6}$$

Similar to equation 3, for a cohesionless soil, the above equation simplifies to:

$$H/V < r.tan\varphi' \quad \text{Equation 2-7}$$

No guidance is provided as to the value of r. The roughness parameter (*r*) can be related to the interface friction angle through the equation below:

$$r = \frac{\tan\delta}{\tan\varphi'} \quad \text{Equation 2-8}$$

Bond and Harris (2009) compared different interface friction angles recommended in different design codes for concrete-soil interface in retaining wall design as shown in Table 2-1. Old British standards (BS 8002) recommend using a value of r = 0.75, while CIRIA guidelines recommend taking the interface friction angle as half or two-thirds of the soil internal friction angle. A more logical guidance is provided in Eurocode 7 (EC7) which takes account of the concrete surface roughness, proposing $\delta = \varphi'$ for cast in-situ concrete and $\delta = \frac{2}{3}\varphi'$ for pre-cast concrete. EC7 also recommends using the constant volume friction angle of the soil, as the soil at the interface may be disturbed or in a loose state after installation.

Table 2-1: Comparison of interface friction angles for different design guidelines for retaining walls (adapted from (Bond & Harris, 2009)

Publication	Surface	Wall friction tan δ	
		Active	Passive
CIRIA 104[13]	any	tan (⅔ φ)	tan (½ φ)
BS 8002[16]	any	¾ tan φ	¾ tan φ
Canadian Foundation Engineering Manual[17]	cast concrete	tan (17–35°)	
	pre-cast concrete	tan (14–26°)	
Eurocode 7	cast concrete	tan (φ_{cv})	tan (φ_{cv})
	pre-cast concrete	tan (⅔ φ_{cv})	tan (⅔ φ_{cv})

Knappett and Craig (2012) also provide useful guidance on choosing the interface friction angle, δ, for different materials. Figure 2-1 shows a direct relationship between δ'/φ' and the ratio of surface roughness (R_a) to mean particle size (D_{50}).

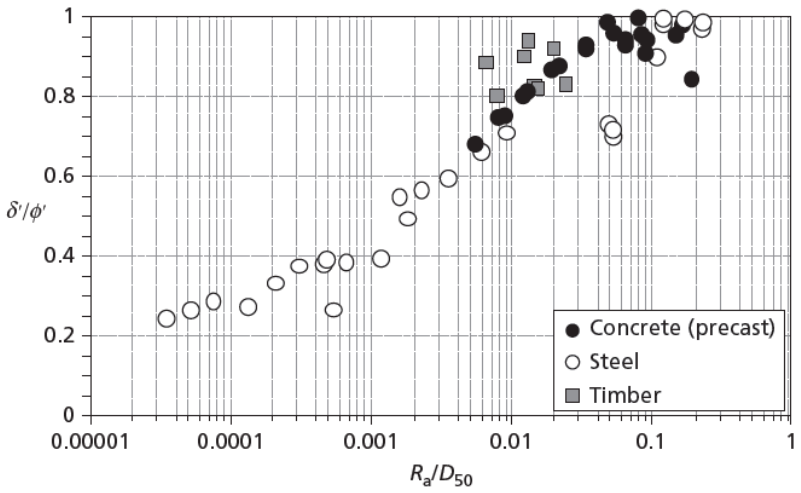

Figure 2-1: Interface friction angle with surface roughness from (Knappett & Craig, 2012)).

Differential settlement is mitigated for in the DNVGL-ST-0126 , "All influences on the structure's response from geometrical tolerances in the construction and from settlements of the soil shall be considered in the design and analysis of the support structure" (DNV-GL, 2018). One of the risks associated with GBFs, due to the reaction of the seabed to their mass is uneven settlement. The permitted accumulated tilt at seabed according to this standard is 0.25°.

2.2 Review of Recent Studies of soil-structure (GBFs) interaction

A recent study by Attari (2016) considered the geotechnical performance of a scaled GBFs model in the field and a calibrated numerical model in Plaxis 3D; it examined the viability of a proposed foundation design using guidelines for offshore foundation codes. It compared a GBF with a piled interface to one without piles. It concluded that the presence of piles improved the sliding resistance, structural stiffness and general structural behaviour during the horizontal loading.

This 2016 study used Tolooiyan and Gavin's (2011) Blessington soil parameters for the Plaxis analysis and used the Hardening Soil (HS) material model. The strength reduction factor (r) for the sand-concrete interface was considered to be approximately 2/3 (0.66). More recent analysis of the same Blessington Sand has revised the relative density (D_r) from 100% to 75% based on Igoe and Gavin's (2019) recent study.

Another recent study by Dunne (2019) conducted with a similar methodology to the laboratory testing in Section 4 i.e. designed to replicate the interface between a gravity base foundation and the seabed using the large shear box machine. Dunne's study assessed the behaviour of a flat based bottom and serrated base for three different soil gradings i.e. Coarse Sand, Gravelly Sand and Sandy Gravel. His paper found that the grading of aggregate used had a direct influence on the shear strength and also friction angle of the interface.

His results suggest that DNV guidelines provide a more optimum design approach based on these tests, indicating that a serrated interface results in upwards of a 30% improvement on horizontal sliding friction compared to that of a smooth interface. It was, however, unclear why the serrated interface over the smooth interface were much less defined for the coarser aggregate grading.

Differential settlement of the GBF will be calculated in Plaxis 3D. Smith et al.'s method (2015) to calculate differential settlement sought to establish different stages of settlement splitting the calculation into three key areas; (i) immediate settlements calculated via traditional analytical methods; (ii) consolidation settlement and rate of consolidation; and (iii) settlement analysis by means of numerical modelling techniques . Settlement results generated in Plaxis and OASYS were compared. The Plaxis set up applied a uniform distributed load (UDL) of 200 kN$/m^2$ over a base plate with 40m diameter. The sand layers were modelled using the Mohr-Coulomb (MC) failure criterion assuming drained condition upon loading.

The initial settlement result of 193mm was questioned by the author as eccentricity of the foundation loading that would result in trapezoidal pressure distribution and with further refinement a differential settlement (ΔS = 135 mm) was achieved. This produced a foundation tilt of the of 0.2°, thus satisfying the criteria adopted of 0.25°at design and 0.75° installation tolerance, giving a total design tolerance of 1°. Smith et al.'s paper (2015) limited itself by using the more basic Mohr-Coulomb (MC) soil model; a more accurate result is expected in the current MAI project by using the HSSmall soil model.

2.3 Finite Element Analysis in Geotechnical Engineering

The use of FEM in geotechnical engineering started in the 1960s. Woodward and Clough (1967) utilised FEM to assess the stress stability and movement in embankments and Reyes and Deane (1966) applied the approach to analyse underground openings in rocks. Its application spread rapidly as advancement in computer power and software improved. It has been a reliable tool in solving geotechnical problems and if employed with proper knowledge and understanding, can carry out realistic predictions, applicable in practical geotechnical problems (Zdravković & Potts, 1999).

Some literature is available on the topic of modelling of gravity base foundations using FEM, Potvin (1990), who analysed the horizontal load-bearing resistance of a skirted GBF using the commercial FEM package Abaqus, also, Murray et al. (1992) and Sturm (2011) carried out important work.

Soil exhibits complicated and nonlinear behaviour, which is influenced by several factors, such as the origin of soil deposits, the grain size, the surrounding environment, the stress history and the load condition among others (Attari, 2016).

2.3.1 Selection of FEM Software

There are a number of commercial and open source options FEM software options available to conduct geotechnical 3DFE analysis e.g. Abaqus, Ansys, PISA, SAFE etc. Some have a good range of analysis possible (linear, non-linear, static, dynamic, construction stages, etc), comprehensive in-built element libraries, good error messaging, high quality meshing techniques, powerful graphical presentation etc. However, there can be issues with relating to having to write scripts externally, more general purpose rather than geotechnical specific, difficult to learn etc.

Plaxis was chosen because it has been in the market for quite some time and there is more academic work evaluated by experts available. Also, it is specific to geotechnical problem solving and has powerful graphical presentation. Although Plaxis does sometime struggle with complex geometry, the GBF in this thesis is relatively straight forward. Plaxis which was developed by Delft University by Brinkgrove, Broere and Watermann allows for theoretically solid computational modelling in a windows-based platform.

2.3.2 Constitutive Soil Model

Numerous constitutive soil models have been developed over the past 40 years for the modelling of stress-strain behaviour of soils. The capabilities and shortcomings of these models are not always easy to ascertain and the requirement for determination of parameters not always uniform. It is consequently difficult to determine which model to select for a particular task (Lade, 2005).

The stress-strain behaviour of soil depends on several factors, namely stress levels, loading direction, anisotropy, rate of loading, drainage and aging (Elhakim, 2005). Constitutive soil models describe the complex stress-strain behaviour of soil.

The degree of accuracy required will determine whether a simple linear elastic-plastic or a more complex method is employed. The simplest available constitutive model is derived from Hooke's law of linear elasticity, and only requires two input parameters, the Young's Modulus (E) and the Poisson's ratio (v) (PLAXIS, 2019).

Constitutive soil models within Plaxis 3D include the Linear Elastic model (LE), Mohr-Coulomb model (MC), Soft Soil model (SS), Hardening Soil model (HS), Soft Soil Creep model (SSC) and

Jointed Rock model (JR). In this thesis, the Hardening Soil small (HSsmall) model has been adopted following the recommendation of Tolooiyan & Gavin (2011)

2.3.2.1 HS Small

The Hardening Soil model with small-strain stiffness (HSsmall) is a modification of the Hardening soil model that accounts for the increased stiffness of the soils at small strains. At low strain levels most, soils exhibit a higher stiffness than at engineering strain levels. And this stiffness varies non-linearly with strain (PLAXIS, 2019).

Two additional material parameters are required G_0^{ref} and $\gamma_{0.7}$. G_0^{ref} is the strain shear modulus and $\gamma_{0.7}$ is the strain level at which the shear modulus id reduced to about 70% of the small-strain shear modulus (PLAXIS, 2019). The HSSmall is the model to be used in section 6 because it gives a more reliable displacement than HS model in working load conditions. Table 2-2 shows the required inputs into Plaxis for a HSsmall soil model.

Table 2-2: Required inputs into Plaxis for a HSsmall soil model (PLAXIS, 2019)

Description	Symbol	Unit
Power for stress level dependency of stiffness	m	[-]
Secant stiffness in standard drained triaxial test	E_{50}^{ref}	kN/m2
unloading / reloading stiffness from drained triaxial test	E_{ur}^{ref}	[kN/m2]
Tangent stiffness for primary oedometer loading	E_{oed}	[kN/m2]
Poisson's ratio for unloading-reloading	V_{ur}	[-]
reference shear modulus at very small strains	G_0^{ref}	[kN/m2]
Threshold shear strain at which G_s = 0.722G_0	$\gamma_{0.7}$	[-]

One feature of soil behaviour that was still missing in the HS-model is the high stiffness at small strain levels, according to Herold & von Wolffersdorff (2009) is the high stiffness at small strain levels (< 10^{-5}).

2.3.3 Interfaces

Interfaces are joint elements to be added to plates or geogrids to allow for proper modelling of soil-structure interaction, they are usually modelled by means of the bilinear MC model (PLAXIS, 2019). A suitable value for the strength reduction factor (R_{inter}) is assigned and can be used as a roughness parameter. Figure 2-2 shows the interface in the Plaxis model to be used in this thesis.

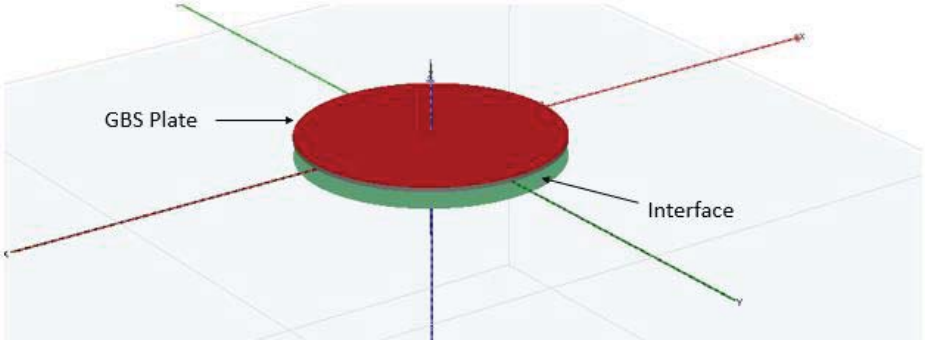

Figure 2-2: Interface plate between soil model and GBS base plate

Understanding ground conditions at the offshore sites help designers establish the most suitable foundation type. Samples from the Blessington test centre has been used by a number of offshore researchers over the past 10 – 12 years: Gavin & O'Kelly (2007) Gavin & Lehane (2005), Igoe, Gavin & O'Kelly, (2011) Gavin and Tolooiyan (2011) and Prendergast et al. (2013) all producing a reliable sets of geotechnical data. The Particle Size Distribution (PSD) is one of the main soil characteristics required. Figure 2-3 shows the Particle Size Distribution (PSD) down to 11.9m below ground level(bgl).

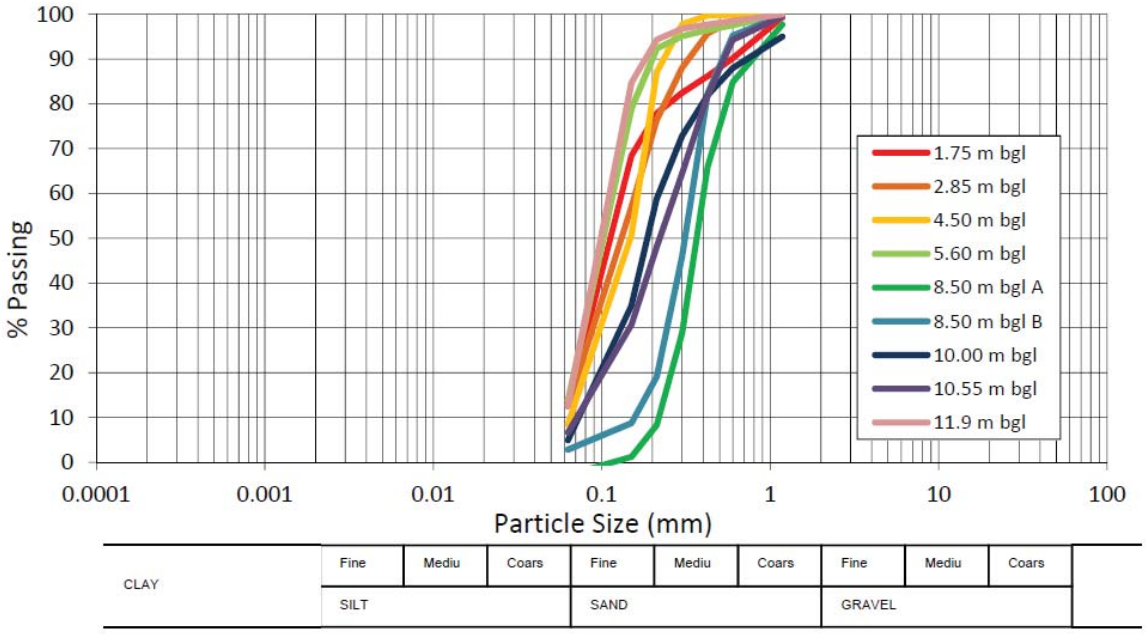

Figure 2-3: Particle Size Distribution at the Blessington test site, after (Doherty, et al., 2012)

2.4 Research Aims and Objectives

The following are the research aims:

- Identify gaps in the offshore design codes in relation to sliding resistance;

- Derive a more refined approach to the calculation of the roughness parameter for the calculation of sliding resistance;
- Quantify how this refined method of calculating the roughness coefficient can reduce GBF ballast requirements;
- Calculate the vertical displacement, lateral displacement and differential settlement of the GBF.

The following are the main research objectives of this thesis:

- Develop an equation based on previous studies to estimate the roughness coefficient (*r*).
- Analyse and interpret laboratory experimental results (commissioned work in Section 4) to establish the roughness coefficients (using equation proposed in Section 2.1) for flat-based and serrated bottoms for range of typical offshore seabed types;
- Determine the reduction in ballast material required from adoption of more refined approach for calculation of sliding resistance (compared to pre-2014 DNV method) based on experimental testing (analytical calculations in Section 5);
- Carry out stability checks by establishing vertical and lateral displacements along with differential settlement for the GBF in Blessington Soil using a 3DFE software (Section 6).

2.5 Literature Review Summary

This thesis aims for more accurate results than Attari's study (2016) using the method of calculation the sliding resistance outlines in Section 2.1 using the Hardening Soil model with small strain stiffness (HSSmall) in Plaxis 3D. J. Dunne's paper (2019) points out a number of shortcomings, namely in the set-up, these will be addressed in the commissioned lab testing in this study (section 4) in an effort to improve the accuracy of the results. Also, an additional soil grading will be added to the lab testing to allow Blessington Sand be assessed. Finally, by applying the constitutive soil model (HS Small) an improvement in the accuracy of Smith et al.'s (2015) work is expected.

The literature review has set out the theoretical framework of this study by outlining the limitations of the current offshore design codes as they apply to bearing capacity and sliding resistance of GBFs and shown how the roughness parameter (*r*) can be related to the interface friction angle. Similar studies that focused in soil-structure interaction have been reviewed with some shortcomings highlighted, this make the case for the importance of this thesis. The evolution and theoretical background of FEM have been outlined illustrating its key role in an in-depth analysis in offshore foundation analysis. Also, the parameters of the soil model (Blessington

Sand) and constitutive soil model (HS Small) used were defined. Finally, the research aims and objectives were defined.

3 Design Basis

This section outlines the design basis for the analytical calculations (Section 5) and finite element modelling exercises (Section 6) in this thesis. It defines the source of the geometry, dimensions, forces, interface parameters and ballast used. It also defines the roughness parameter (*r*) friction angles and factors of safety to be used. All assumptions associated with each value are outlined.

3.1 Design Basis Parameters for Ballast Material Analysis

Section 5 of this thesis demonstrates how a reduction on ballast material required can be achieved from the adoption of a more refined approach for calculation of sliding resistance through a preliminary design example for a gravity base foundation supporting an offshore wind turbine in 45m water depth (11 cases studied ranging from 15 kTonne to 40 kTonne). As calculating the loading on the GBF was not part of the objectives the values were mostly extracted from similar projects. The turbine interface loads were selected based on reference loads for the Rotor Nacelle Assembly (RNA) of the 10MW DTU offshore wind turbine (Bak, et al., 2013), Table 3-1 provides a summary of these weights. Section 5 will compare the pre-2014 method of calculation bearing, sliding and overturning with the more refined approach suggested in section 2.1.

Table 3-1: Key weigh parameters DTU 10 MW RNA

DTU 10 MW Key Weight parameters	
Rotor Mass	227.962 T
Nacelle Mass	446.036 T
Tower Mass	628.424 T
Total	**1302.422 T**

The geometry of the gravity base foundation, water depth, maximum horizontal force and overturning moment were adopted from on ARUP's GRAVITAS GBF design (Smith, et al., 2015). Figure 3-1 gives an illustrative representation of the geometric and loading assumptions to be used in the ballast material analysis in (Section 5).

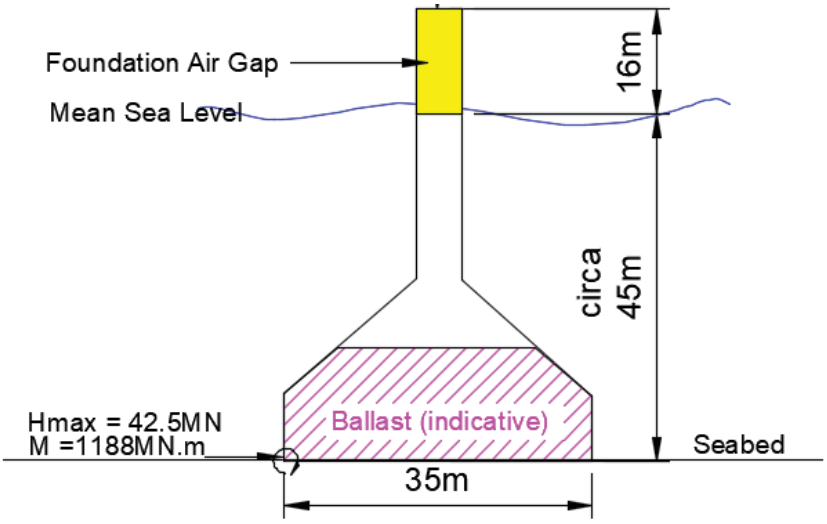

Figure 3-1: Geometric and loading assumptions (Smith, et al., 2015)

Vertical resultant force at the base

To estimate the vertical resultant force at the GBF base (including buoyancy) for each case is the all downward and upward forces are required. Table 3-2 presents the source and values used in the calculation of the vertical resultant force at the base of the GBF.

Table 3-2: Calculation of the vertical resultant force at the base of the GBF

Description	Source	Value	unit
Net concrete volume	ARUP's Gravitas GBF (Smith, et al., 2015)	3000	m^3
Height of conical section of BGF	ARUP's Gravitas GBF (Smith, et al., 2015)	25	m
RNA weight	DTU 10 MW (Bak, et al., 2013)	1302	Tonne
Buoyancy	ARUP's Gravitas GBF (Smith, et al., 2015)	-16	MN
Ballast (11 cases)	---	15 to 40	kTonne
Vertical Resultant Force		**14.389 - 340.009**	**MN**

Equation 3-1 shows the formula used:

Ballast + GBF + RNA – upward buoyancy force Equation 3-1

Equation 3-1 shows how the vertical resultant force was calculated. The example used is for 30 kTonnes of ballast (mid-range). A reduction factor is applied to account for the reduction of BGF from 40m to 35m.

=3000x25x$(35/40)^2$/1000 + 30x9.81 + 1302x9.81/1000-16x$(35/40)^2$ Equation 3-2

H = 241.99 MN

Horizontal resultant force at the base

The horizontal resultant force is calculated using the in Smith et al.'s paper (2015) and environmental loads as shown in Table 3-3.

Table 3-3: Calculation of the horizontal resultant force at the base of the GBF

Description	Source	Value	unit
Horizontal Force on GBF	ARUP's Gravitas GBF (Smith, et al., 2015)	38	MN
Correction for scaling up from a 6MW to a 10MW turbine	---	4.5	MN
Horizontal resultant force (H_{max})		**42.5**	**MN**

Moment

The moment is calculated using the following formula:

=Horizontal load on GBF + correction load x (air gap +water depth + distance to RNA hub) Equation 3-3

Table 3-4: Calculation of the moment at the base of the GBF

Description	Source	Value	unit
Overturning moment	ARUP's Gravitas GBF (Smith, et al., 2015)	450	MNm
Correction for scaling up from a 6MW to a 10MW turbine	---	4.5	MN
Distance from seabed to mean sea level	ARUP's Gravitas GBF (Smith, et al., 2015)	45	m
Distance from turbine hub to mean sea level	ARUP's Gravitas GBF (Smith, et al., 2015)	103	m
Air gap	ARUP's Gravitas GBF (Smith, et al., 2015)	16	m

Hub height	DTU 10 MW (Bak, et al., 2013)	119	m
Moment (M)		**1188**	**MNm**

The (M) value are calculates as follows:

450 + 4.5 x (16+45+(119-16) Equation 3-4

M= 1188 MNm

Table 3-5: Summary table of loading values used in Section 5 – ballast material analysis

Description	Symbol	Value	unit
Horizontal resultant force at the base	*H*	42.5	MN
Vertical resultant force at the base	*V*	14.389 - 340.009	MN
Overturning Moment	*M*	1188	MN.m

The seabed is assumed to be comprised of as coarse SAND to gravelly SAND sediments with a constant-volume friction angle (ϕ_{cv}) of 35 deg.

The formula used to calculate the bearing capacity was obtained from the DNV-GL codes (DNV-GL, 2014):

$$q_d = \frac{1}{2}\Upsilon' b_{eff} N_\Upsilon s_\Upsilon i_\Upsilon + p'0 N_q s_q i_q + c_d N_c s_c i_c$$ Equation 3-5

Where:

q_d design bearing capacity (kN/m^2)

Υ' effective (submerged) unit weight of soil (kN/m^3)

$p'0$ effective overburden pressure at the level of the foundation-soil interface (kN/m^2)

c_d design cohesion assessed on the basis of the actual shear strength profile, load configuration and estimated depth of potential failure surface (kN/m^2)

N_Υ, N_q, N_c bearing capacity factors, dimensionless

s_Υ, s_q, s_c: shape factors, dimensionless

i_Υ, i_q, i_c: inclination factors, dimensionless

q overburden pressure at the level of the foundation-soil interface (kN/m^2)

To differentiate between the DNV-pre 2014 method and the approach proposed by this thesis two different roughness factor (*r*) of were used as outlined in Table 3-6. The pre-2014 r-value was calculated using the following equation:

$$0.4/\tan(\phi') = 0.57 \qquad \text{Equation 3-6}$$

And the (r) used in this thesis will be based on lab results.

Table 3-6: Roughness parameters used in analytics analysis

Approach	Source	Roughness Parameter (r)
Pre 2014 method	(DNV-GL, 2014)	0.57
Proposed refined approach in this MAI (from lab. experiment results)	Section 4	Based on Lab results

The factors of safety (FoS) to be used are outlined in Table 3-7. For the purpose of comparison, the FoS will be expressed as the "FoS utilisation" which is calculated as the available FoS divided by the minimum required FoS, values are based on the American Petroleum Institute's (API, 2007) recommendations.

Table 3-7: Minimum overall FoS and FoS utilisation assumed for different design checks

Description	Minimum FoS Value	FoS Utilisation (%)
Bearing Capacity FoS	2.0	FoS/minimum FoS required
Sliding Resistance FoS	2.0	FoS/minimum FoS required
Overturning FoS	1.5	FoS/minimum FoS required

3.2 Design Basis for Finite Element Analysis in Plaxis

The Plaxis model will be set up with project dimensions of 100m x 100m and a depth of -80m bgl to allow sufficient space for any deformation to take place within those boundaries.

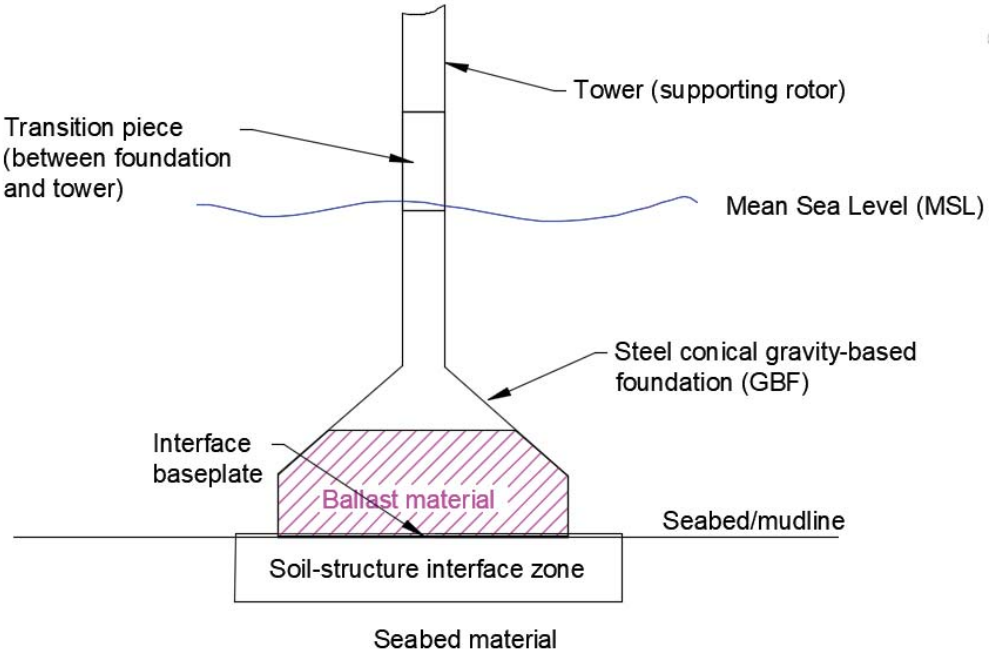

Figure 3-2: General elements GBF and terms used in the Finite Element Analysis (Section 6)

3.2.1 Soil model

The Plaxis soil model is based on Blessington Sand. Hardening Soil with small-strain stiffness (HSsmall) models will be the constitutive soil model used (reviewed in Section 2.3). HS model is an advanced model that demonstrates the relationship between the stress and strain in the soil using a hyperbolic function (Jalali, et al., 2012). HSsmall accounts for the increased stiffness of the soils at small strains. At low strain levels most soils exhibit a higher stiffness than at engineering strain levels, this stiffness varies non-linearly with strain (PLAXIS, 2019). A HSsmall material soil model was applied and drained conditions assumed.

A summary of the assigned soil material properties to the Plaxis model are outlines in the following section.

The peak friction angle was obtained from Bolton's 1986 paper (Bolton, 1986) using the following formula:

$$\psi = (\varphi_{cv} - \varphi_{cv})/0.8 \qquad \text{Equation 3-7}$$

The φ_{cv} of 33° was derived from the lab results as outline in Figure 4-15 in section 4.

(40 – 33)/ 0.8 = 8.75°

The relative density (D_r) was used to assign a stiffness to the soil model. A D_r of 75% was assumed based results from the characterisation of Blessington soil (Igoe & Gavin, 2019). Figure 3-3 is a graph of this D_r with respect to depth and the 75% assumed.

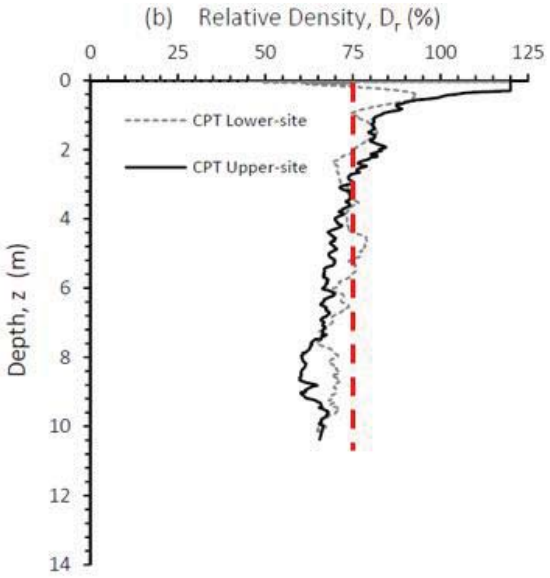

Figure 3-3: Relative density vs depth at Blessington (Igoe & Gavin, 2019)

The relative density is also used to calculate the effective stress (ϕ') from using the following formula (Brinkgreve, et al., 2010):

$$\phi' = 28 + 12.5D_r/100 \qquad \text{Equation 3-8}$$

The reference stiffness parameters E_{50}^{ref}, E_{50}^{ref} and E_{oed} were reviewed in Section 2.3.2.1. The values to be used in Plaxis base on the formula suggested by Brinkgreve in his 2010 paper "validation of empirical formulas to derive model parameters for sands" (Brinkgreve, et al., 2010)

The triaxial loading stiffness formula is:

$$E_{50}^{ref} = 60000\ D_r/100 \text{ [kN / m}^2\text{]} \qquad \text{Equation 3-9}$$

$$E_{50}^{ref} = 45{,}000 \text{ kN / m}^2$$

The oedometer loading stiffness formula is:

$$E_{oed}^{ref} = 60000\, D_r/100 \text{ [kN / m}^2 \qquad \text{Equation 3-10}$$

$$E_{oed}^{ref} = \qquad 45{,}000 \text{ kN / m}^2$$

The triaxial unloaded stiffness formula in the same publication is:

$$E_{ur}^{ref} = 108000 + 68000\, D_r/100 \text{ [kN / m}^{2]} \qquad \text{Equation 3-11}$$

However, three times the value equation 3-5 was used.

$$E_{ur}^{ref} = \qquad 135{,}000 \text{ kN / m}^2$$

The actual stiffness is stress-dependent. The rate of stress dependency (m) is observed to be negatively correlated with the density. The following formula is proposed for m, as suggested by Brinkgreve (2010):

$$m = 0.7 - D_r/320 = 0.465 \qquad \text{Equation 3-12}$$

Brinkgreve et al. suggests a Poisson ratio for unloading and reloading, V_{ur}, of 0.2 (Brinkgreve, et al., 2010).

G_0^{ref} and $\gamma_{0.7}$ are two additional material parameters required for HSS. G_0^{ref} is the strain shear modulus and $\gamma_{0.7}$ is the strain level at which the shear modulus is reduced to about 70% of the small-strain shear modulus (PLAXIS, 2019). These two values were also obtained from Brinkgreve (Brinkgreve, et al., 2010) using the following formulae:

$$G_0^{ref} = 60000 + 68000\, D_r/100 \qquad \text{Equation 3-13}$$

$\gamma_{0.7}$ = (2-D_r/100) *10^{-4} Equation 3-14

A summary of all parameters used in Plaxis is proved in Table 3-8.

Table 3-8 – Summary table of HSsmall parameters

Description	Symbol	Value	Unit
Effective submerged unit weight	Υ_{sat}	20	kN/m3
Peak friction angle	[Ψ]	8.75	[°]
Relative density	D_r	75	%
Effective stress	ϕ'	35	[°]
Secant stiffness in standard drained triaxial test	E_{50}^{ref}	45,000	kN/m2
Unloading / reloading stiffness from drained triaxial test	E_{ur}^{ref}	45,000	[kN/m2]
Tangent stiffness for primary oedometer loading	E_{oed}	135,000	[kN/m2]
Power for stress level dependency of stiffness	m	0.465	[-]
Poisson's ratio for unloading-reloading	V_{ur}	0.2	[-]
Reference shear modulus at very small strains	G_0	150,000	[kN/m2]
Threshold shear strain at which G_s = 0.722G_0	$\gamma_{0.7}$	0.0001	[-]

3.2.2 Base Plate Properties

The model required the base plate to be extremely stiff. To ensure this a high stiffness values was assigned to the base plate material 20.00 x 10^9 kN/m2; ten times that of steel to ensure no deformation or buckling during calculations. Table 3-9 shows the properties of the base plate to be used.

Table 3-9: Base plate properties

Description	Symbol	Value	Unit
Material Type	---	Elastic	---
Depth	d	10	m

Young's Modulus	E_1	20.00 x 10^9	kN/m2
Shear Modulus	G_{12}	10.00 x 10^9	kN/m2

3.2.3 Loading Applied to Base Plate

In Plaxis the GBF was designed as a surface plate with point loads and moments applied. The geometry of the gravity base foundation and hydrodynamic loads were adopted from (Smith, et al., 2015). The turbine interface loads were selected based on reference loads for a 10MW DTU offshore wind turbine (Velarde, 2016)(see Table 3-5). These values will be used in the analysis in Section 5 to allow comparisons and verifications.

The base diameter to be used is 35m. The maximum vertical resultant forces will correspond the values used for the ballast values of 20kT, 30kT and 40kT used in Section 6; 14389 kNm, 24199kNm and 34009kNm respectively. The moment applied will be 118800 kNm

3.2.4 Interface

Below the base plate and above the soil an interface plate was created to mimic the serrated based bottom (reviewed in Section 2.3.3). An R_{inter} = will be assigned based on the roughness coefficinet (r) results of the lab testing in Section 4.

3.3 Summary of Values Used in Calculations

Table 3-10: Comment on inter-relationship of values and calculations used in main sections of this thesis

	Section 2 (Literature Review)	Section 3 (Design Basis)	Section 4 (Lab. testing)	Sections 5 (Worked Example)	Section 6 (3DFE)
GBF Geometry	---	ARUP's GBF design defined	---	Based on Design Basis Section 2.1	Based on Design Basis Section 2.2
Baseline offshore wind turbine	---	DTU 10MW OWT defined	---	DTU 10MW turbine forces	DTU 10MW turbine forces
Interface Type	---	Smooth and Serrated base defined	Smooth and Serrated base	Only serrated base analysed	Only serrated base analysed

Refined roughness coefficient (*r*)	Refined approach Defined (Equation 2-8)	Pre-2014 method defined	Equation 2-8 used (*r*)	Used result of refined approach (*r*) value from lab. testing.	Used result of refined approach (*r*) value from lab. testing.
Pre-2014 roughness parameter (*r)*	---	---	---	Compared pre-2014 method to estimate (*r)* against refined approach	---
Ballast	---	---	---	15 – 40kT	20, 30 & 40 kTonne
Loading/ Hydrodynamic Forces	---	Defined loading used in Sections 5 & 6	100 kPa, 200 kPa & 300 kPa	Used values defined in Section 3.1	Used values defined in Section 3.2
Seabed type/ Soil grading	---	Plaxis soil model defined Section 3.2.1	Range of soils with PSDs defined in Figure 4-4	Range of soils with PSDs defined in Figure 4-4. Fine grained SAND to sandy GRAVEL).	Soil model defined in Section 3.2.1
FoS	---	API FoS values defined (Table 3-7)	---	API FoS values used (Table 3-7)	Plaxis FoS values Used

4 Laboratory Testing and Interpretation

The laboratory testing phase of this industry-based MAI project was commissioned by Gavin and Doherty Geosolutions Ltd (GDG) as part of work carried out for the SEAI. The design of the experimental work and, in particular, the addition of Blessington sand as a soil grading was instigated by the author of this thesis. Experiments were carried out by the lab technician and supervised by Dr. David Igoe.

Analysing sliding resistance in a series of shear box tests were undertaken using large shear box apparatus in the Geotechnical Laboratory in the department of Civil, Structural and Environmental Engineering at Trinity College Dublin.

This section provides the details of methodology including interface geometries considered and soil gradings used, as well as, the results obtained including variation in sliding resistance with increasing vertical load and associated interface friction angles.

4.1 Laboratory Testing Objectives

A series of large shear box tests were undertaken in order to provide estimation of interface friction for different GBF interface types and soil gradings. The objective of the study is to provide insight into underlying mechanisms/phenomena that contribute to the sliding resistance of conventional concrete GBF interface and to investigate upper and lower bound interface friction for a range of soil gradings.

The following laboratory tests were undertaken using a large shear box setup with dimensions 300 x 300mm

- 12 no. tests with soil-soil interface
- 12 no. tests with soil-smooth concrete interface
- 12 no. tests with soil-ridged concrete interface

4.2 Laboratory Testing Methodology

4.2.1 Large Shear box apparatus

The large shear box apparatus, shown in Figure 4-1, tests a sample which measures 300mm x 300mm in plan, with a maximum sample depth of 200mm. The box section of the apparatus is split in half, with the bottom half allowing horizontal movement, with the top reacting against a

proving ring to measure the shearing load. The loading arm applies the normal force in the sample via the loading plate, which is controlled hydraulically. The loading plate sits within the box section, and ensures the load is uniformly distributed over the sample. Vertical and horizontal displacement are measured during the testing using Linear Variable Differential Transformers (LVDTs) as shown in Figure 4-2.

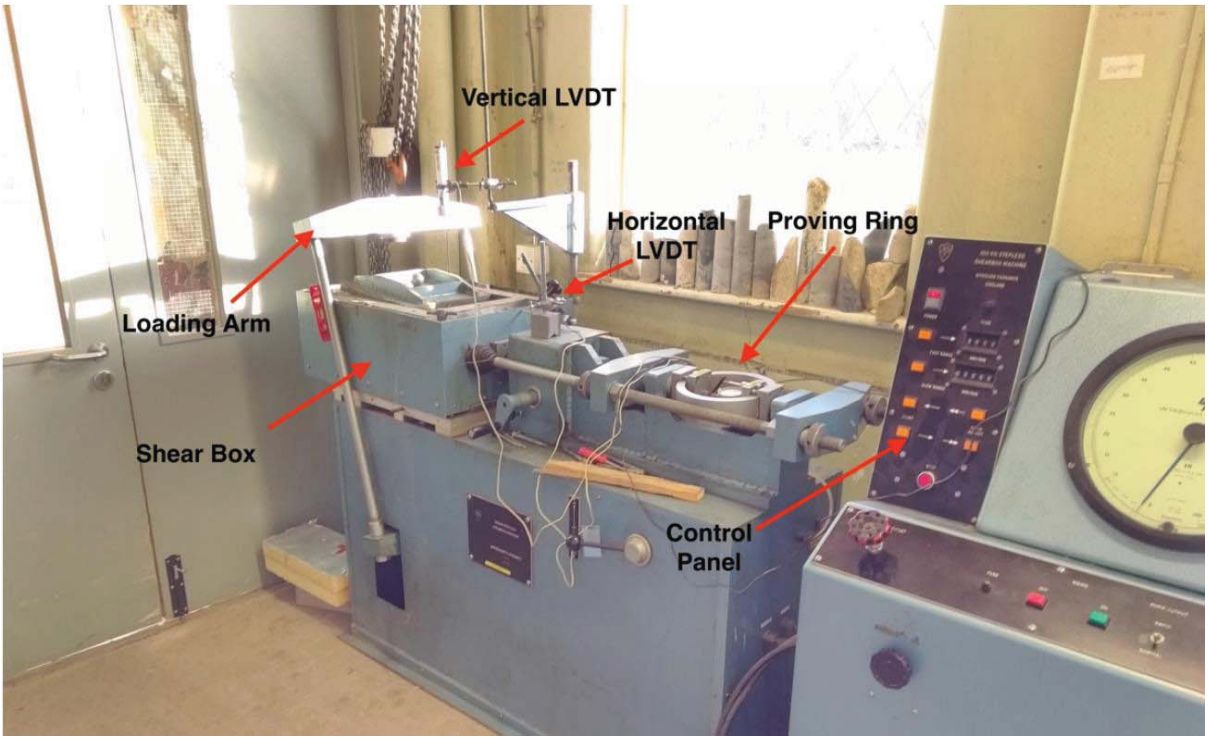

Figure 4-1: Large shearbox apparatus at Trinity College Dublin

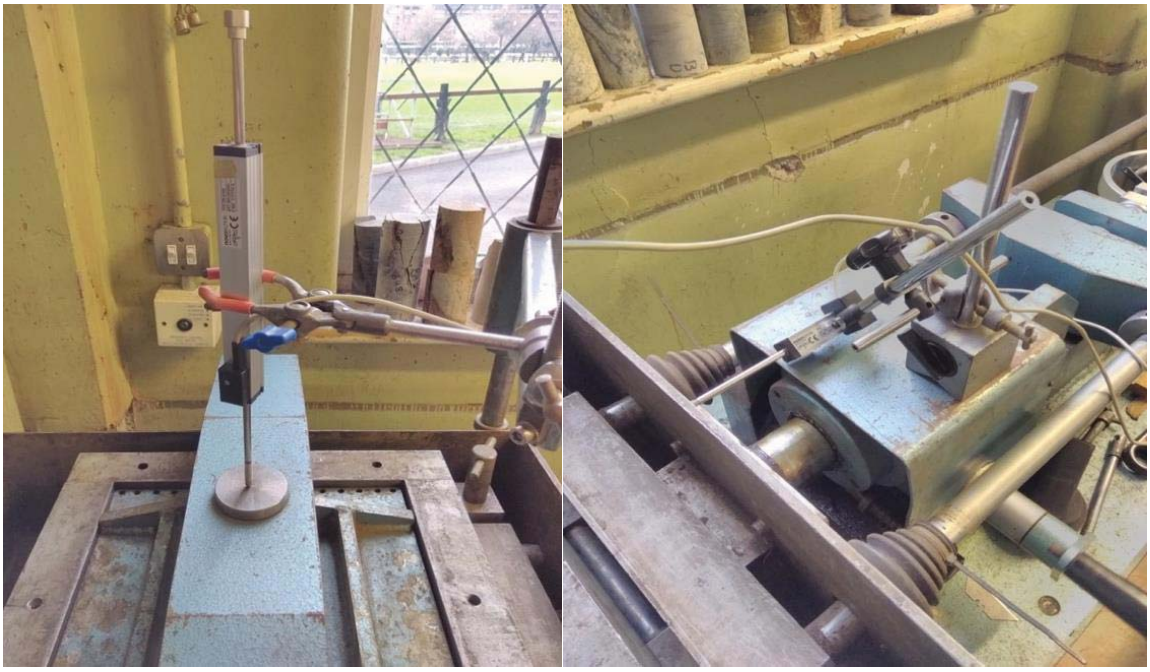

Figure 4-2: (a) Vertical and (b) horizontal LVDTs

Figure 4-3 shows the calibration of proving ring using Denison Universal Testing Machine.

Figure 4-3: Calibration of proving ring using Denison Universal Testing Machine

4.2.2 Aggregate Preparation

Four different aggregate sizes to test, with a range of fine, medium and coarse sands and gravels used during the testing. Gradings 1 - 3 were manufactured from crushed aggregate sourced from Roadstone's quarry in Belgard, Co. Dublin. The particle sizes varied between 20mm (maximum recommended in large shear box) and 0.1mm and were designed to represent a coarse sand (grading 1), a sandy gravel (grading 2) and a clean gravel (grading 3) deposit. Due to the fact that gradings 1 – 3 were made from crushed aggregate, the particles have a higher angularity and lower sphericity than typical natural sands and gravels, and thus have high internal friction angles. For this reason, grading 4 was selected as a natural fine sand, from the Roadstone Redbog quarry in Blessington, Co. Wicklow, and was not manufactured. The particle size distribution for the four gradings are shown in Figure 4-4 and demonstrate the range of particle sizes covered.

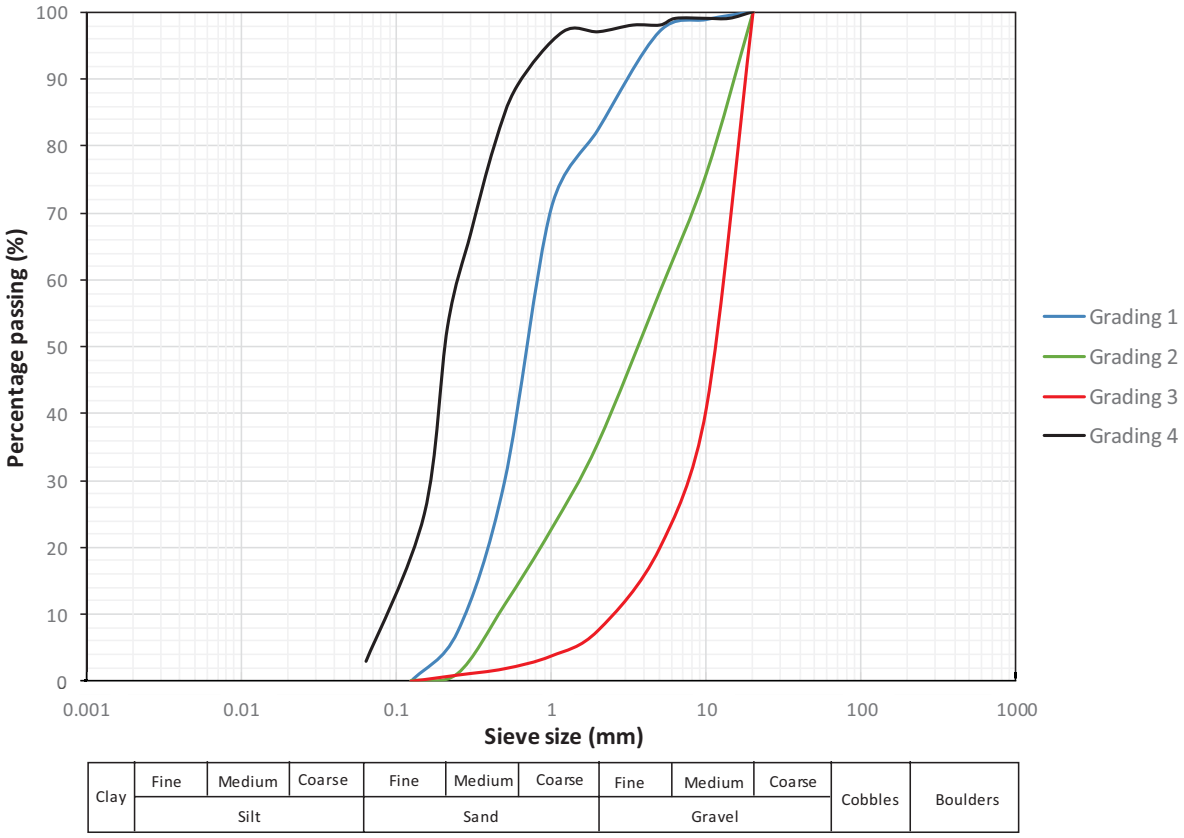

Figure 4-4: Particle Size Distribution (PSD) of the four different gradings tested

The process for preparing gradings (1 -3) into their three separate gradings, based on the PSD involved the following (shown in Figure 4-5):

1. The aggregates were washed to remove unwanted dirt and dust and then over dried for 24 hours.
2. The aggregates were then sieved and grouped according to particle size using a mechanical sieve shaker, weighing each size and separating them based on the required amount for each of the three gradings.
3. The samples were then mixed thoroughly and then loosely placed in the shear box for testing.

Figure 4-5: (a) Washing, (b) drying and (c) sieving of aggregates for preparing gradings 1-3

4.2.3 Concrete Interfaces

Two concrete interface plates were required for the testing, of dimensions 300mm x 300mm x 100mm, to match that of the large shear box. The initial mix design process involved ensuring the correct water/cement ratio and fine/coarse aggregate ratio would result in the required strength. In order to ensure a high strength mix would be obtained, the water to cement ratio was limited to 0.3. As a result, a superplasticiser was added to the mix to ensure the mix was still workable, which was particularly important for the serrated interface plate so that the concrete mix uniformly spread throughout the formwork. The exact quantities and ratios of each material used are shown Table 4-1.

Table 4-1: Concrete mix used for concrete interfaces

Material (Unit)	Quantity
Cement (kg/m3)	760
Water (l/m3)	250
Fine Aggregate - 2mm (kg/m3)	620
Coarse Aggregate - 5mm (kg/m3)	725
Superplasticiser (ml/m3)	8000

For the ridged concrete interface, the dimensions are shown in Figure 4-6. These ridges were created using a timber formwork mould in the engineering labs at TCD.

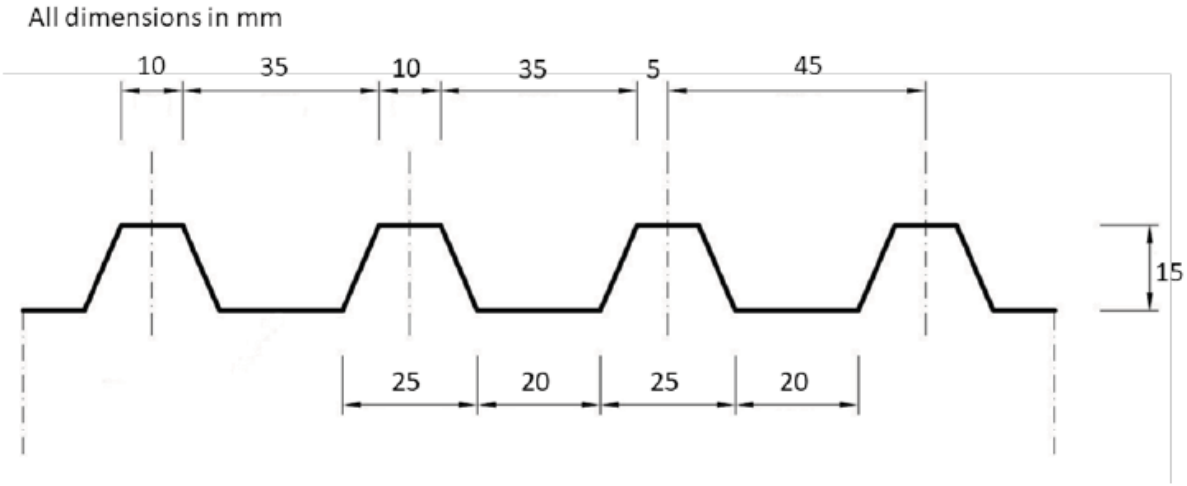

Figure 4-6: Dimensions of ridges for ridged concrete interface

In making the concrete mix for this smooth interface plate, enough materials were used to make interfaces and 6 cubes for strength testing. The concrete was mixed and added to the interface formwork as well as the cube moulds and then vibrated to ensure a compact mix and minimum entrapped air. Both concrete interfaces are shown in Figure 4-7.

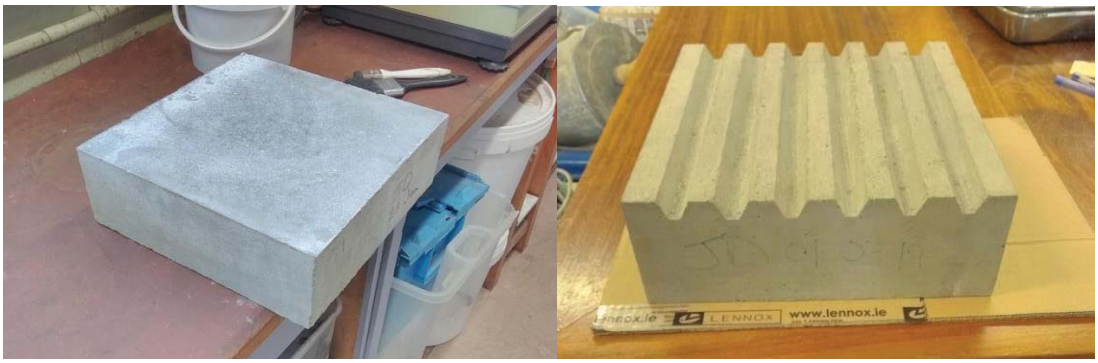

Figure 4-7: Concrete Interfaces used in testing

The concrete cubes were cured in a water bath at 20 degrees Celsius and tested at 7, 14 and 28 days (Figure 4-8). A concrete compressive strength of >75 MPa was achieved after 7 days, 84 MPa after 14 days and 91 MPa achieved after 28 days. This was more than sufficient for the required testing.

Figure 4-8: Concrete cube testing in Toni Technik Compression Machine

4.2.4 Concrete Interface Testing Methodology

All the Proving rings and LVDTs were calibrated prior to commencing testing. For the soil-soil and concrete interface testing a shear rate of 3 mm/min. In conducting each test, the following steps were taken:

1. The interface was added to the bottom half of the machine (Figure 4-9a and Figure 4-10a).

2. The aggregate grading was added on top of the plate (Figure 4-9b and Figure 4-10b).

3. The loading plate added to the top of the shear box.

4. The surcharge pressure was applied, beginning with 100kPa.

5. The shear rate was set to 3mm/min.

6. The test ran for approximately 13 minutes – more than enough to ensure that the horizontal strain reached at least 10% (30mm).

7. The machine was stopped and the test data extracted

(a): Flat Interface Plate placed in the Shear Box

(b): Grading #3 (coarse) placed on top of the Plate

Figure 4-9: Smooth concrete interface test setup

(a): Serrated Interface Plate in the Shear Box

(b): Grading #1 Placed on top of the Serrated Interface

Figure 4-10: Ridged concrete interface test setup

4.2.5 Test List

A total of 36 concrete interface tests were undertaken. The details of each test are provided in Table 4-2 .

Table 4-2: List of concrete interface tests

Test No.	Test ID	Interface	Soil Grading	Normal Stress [kPa]
1	G1SO100	Soil - Soil	1	100
2	G1SO200	Soil - Soil	1	200
3	G1SO300	Soil - Soil	1	300
4	G2SO100	Soil - Soil	2	100
5	G2SO200	Soil - Soil	2	200
6	G2SO300	Soil - Soil	2	300
7	G3SO100	Soil - Soil	3	100
8	G3SO200	Soil - Soil	3	200
9	G3SO300	Soil - Soil	3	300
10	G4SO100	Soil - Soil	4	100
11	G4SO200	Soil - Soil	4	200
12	G4SO300	Soil - Soil	4	300
13	G1P100	Smooth Concrete	1	100
14	G1P200	Smooth Concrete	1	200
15	G1P300	Smooth Concrete	1	300
16	G2P100	Smooth Concrete	2	100
17	G2P200	Smooth Concrete	2	200
18	G2P300	Smooth Concrete	2	300
19	G3P100	Smooth Concrete	3	100
20	G3P200	Smooth Concrete	3	200
21	G3P300	Smooth Concrete	3	300
22	G4P100	Smooth Concrete	4	100
23	G4P200	Smooth Concrete	4	200
24	G4P300	Smooth Concrete	4	300
25	G1T100	Ridged Concrete	1	100
26	G1T200	Ridged Concrete	1	200
27	G1T300	Ridged Concrete	1	300
28	G2T100	Ridged Concrete	2	100
29	G2T200	Ridged Concrete	2	200
30	G2T300	Ridged Concrete	2	300
31	G3T100	Ridged Concrete	3	100
32	G3T200	Ridged Concrete	3	200
33	G3T300	Ridged Concrete	3	300
34	G4T100	Ridged Concrete	4	100
35	G4T200	Ridged Concrete	4	200
36	G4T300	Ridged Concrete	4	300

4.3 Laboratory Testing Results

This section provides a summary of the main results.

4.3.1 Concrete Interface Test Results

Plots of maximum shear stress vs normal stress and friction angle vs normal stress are provided for the concrete tests for each grading below in Figure 4-11 to Figure 4-14. The friction angle for the finest gradings (grading 4) varies from 30 – 34 degrees. The friction angle for the coarsest grading (grading 3) shows a much larger variation in friction angle from 30 – 53 degrees depending on the interface, with soil-soil tests providing the largest friction angles.

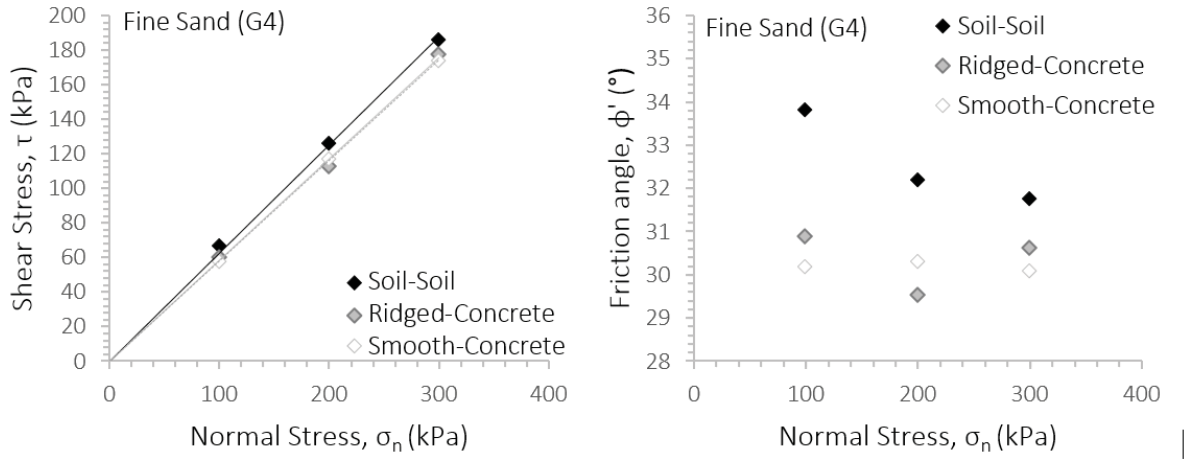

Figure 4-11: Summary results for concrete tests Grading 4

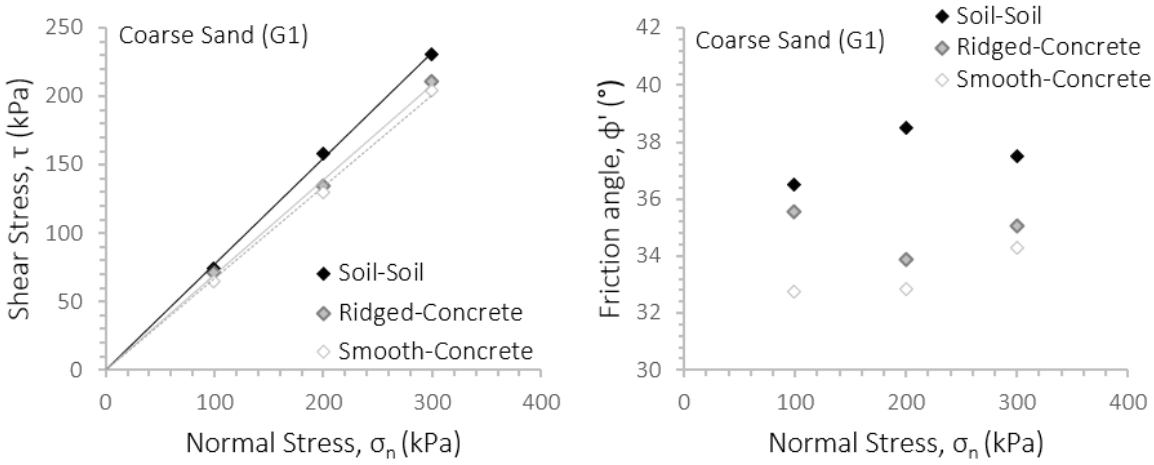

Figure 4-12: Summary results for concrete tests Grading 1

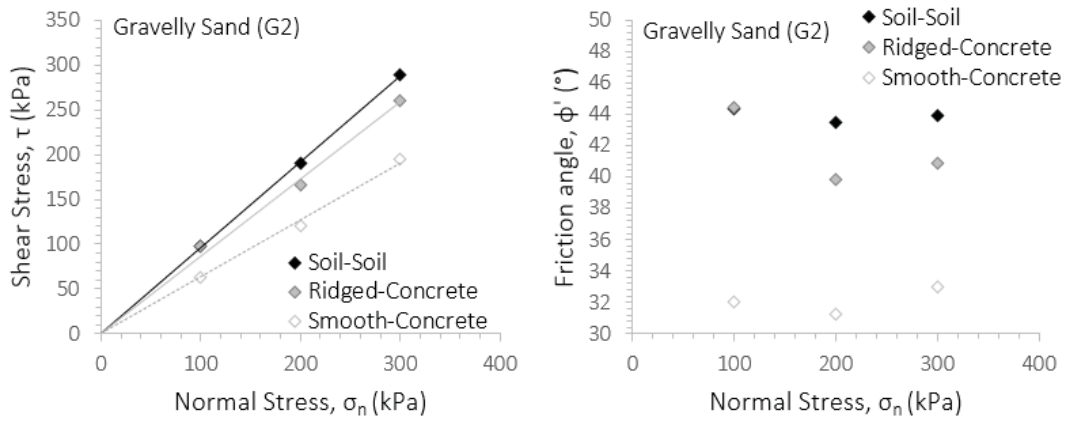

Figure 4-13: Summary results for concrete tests Grading 2

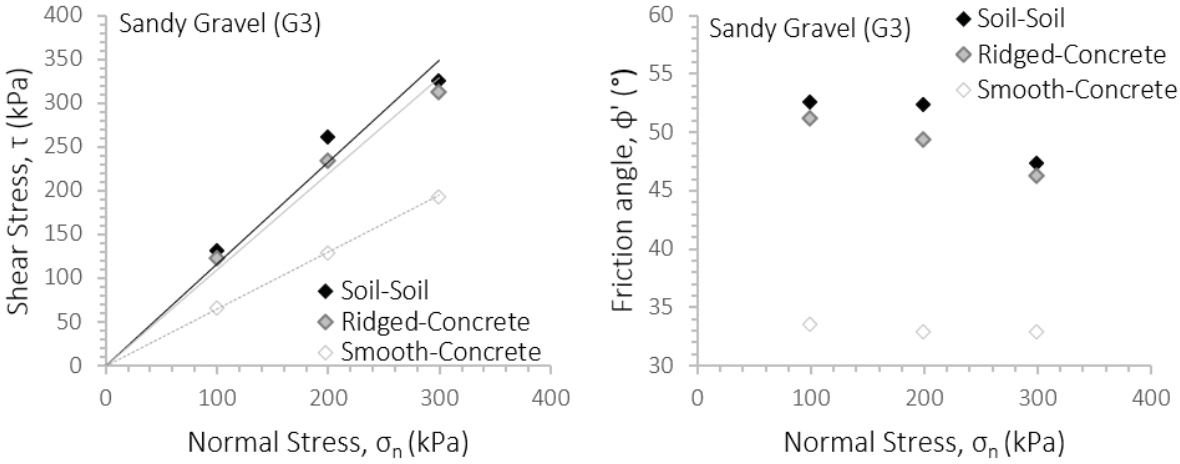

Figure 4-14: Summary results for concrete tests Grading 3

4.3.2 Concrete Interface Interpretation

A comparison of the interface friction angles for different gradings and interfaces is provided in Figure 4-15. It is evident that the soil grading has a strong impact on the friction angle developed in soil – soil tests, with larger particle sizes showing higher friction angles (grading 3 – gravel shows the largest friction angle for soil-soil tests, grading 4 – fine sand shows the lowest friction angles). The ridged concrete interface tests show a broadly similar trend to that of the soil – soil tests but with slightly lower friction angles. The smooth concrete interface tests provide lower interface friction angles of 30 – 34 degrees and are relatively insensitive of soil grading. The results show that the friction angles are highly dependent on particle size, as well as soil grading.

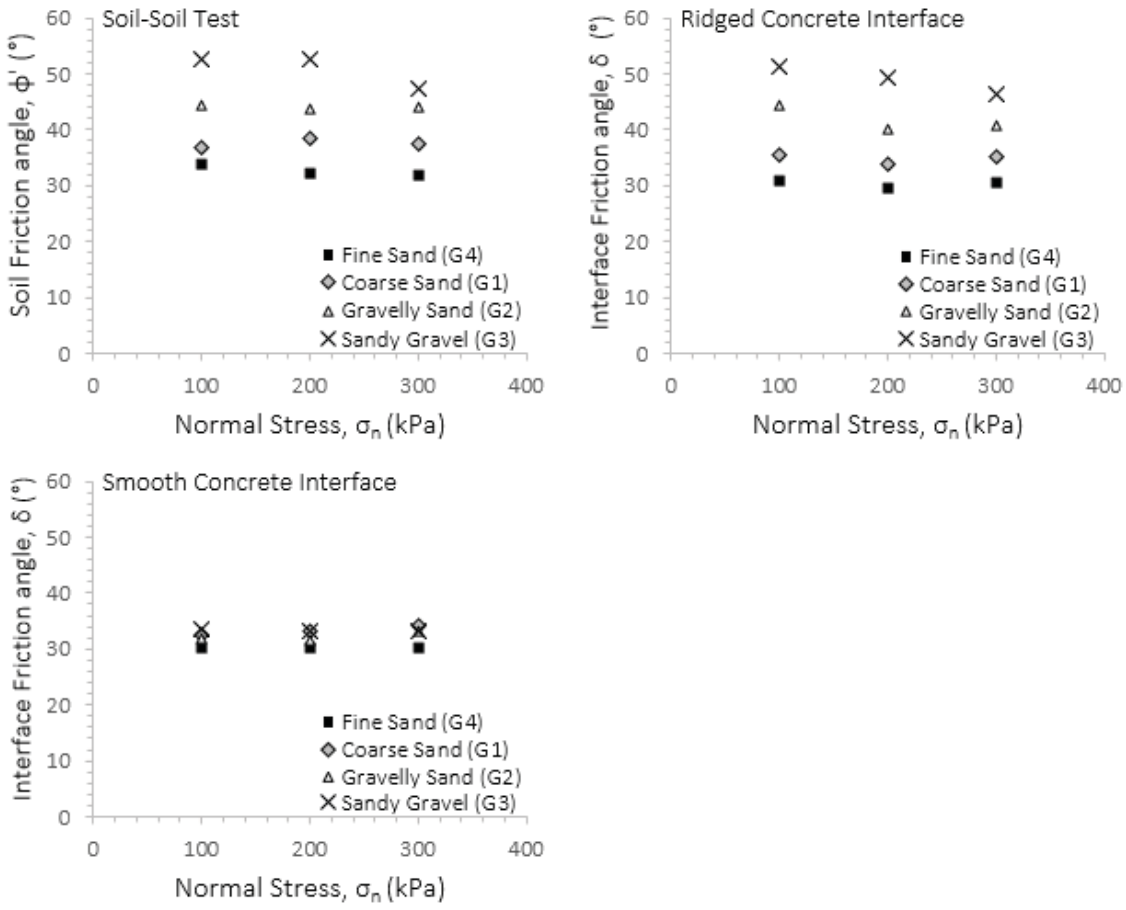

Figure 4-15: Friction angle comparison between different gradings for (a) soil-soil tests (b) ridged-concrete tests and (c) smooth-concrete tests

A comparison of the roughness coefficients (*r*) (defined in 2.1), for the two concrete interfaces is shown in Figure 4-16. The roughness coefficient (*r*) for the ridged concrete interface is seen to vary from a lower-bound of 0.85 to a maximum value of 1.0 and is relatively independent of soil grading. For the smooth concrete interface, the roughness coefficient (*r*) shows much larger variation from a lower-bound value of 0.5 to an upper-bound of 0.95, and is highly dependent on soil grading. The lowest roughness coefficient for the smooth concrete interface occurs for the largest particle sizes (grading 3).

It should be noted that the low roughness coefficient measured for the smooth-concrete with grading 3 is a result of the high soil-soil friction angles from the grading 3 tests, as the actual interface friction angles developed for the smooth concrete tests were similar and independent of soil grading (see Figure 4-15c).

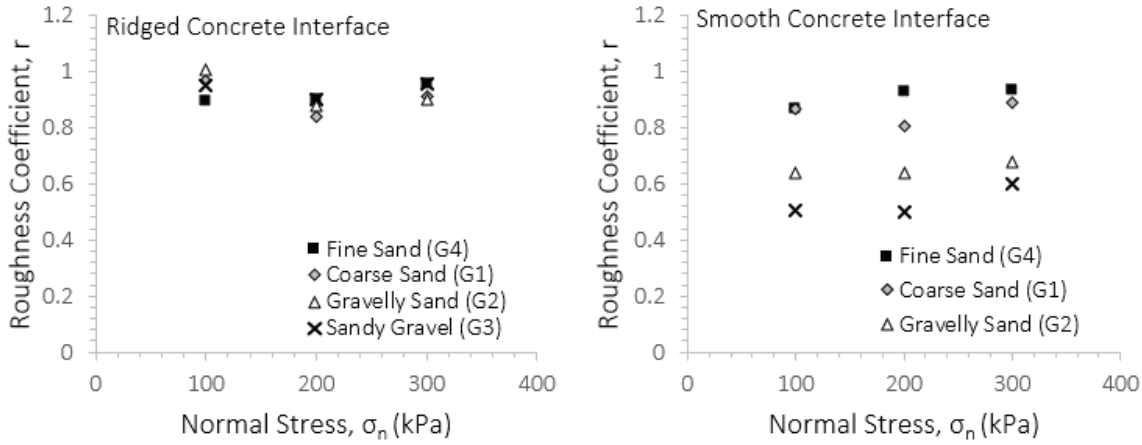

Figure 4-16: Interpretation of roughness coefficient (r) for (a) ridged concrete interface and (b) smooth concrete interface

5 Ballast Material Analysis

5.1 Methodology

This section demonstrates cost saving (in the form of a reduction in ballast material requirements) that can be achieved from the adoption of more refined approach for calculation of sliding resistance, bearing capacity and overturning through a preliminary design example for a GBF supporting an offshore wind turbine in 45 m water depth. The geometry of the GBF, water depth, and hydrodynamic loads were adopted from an ARUP based design (Smith, et al., 2015). The turbine interface loads were selected based on reference loads for a 10MW DTU offshore wind turbine. All design basis and calculations for values used in this section can be found in Section 3.1. with a summary table of loads and overturning moment applied to the gravity base foundation at the mudline level are provided in Table 3-5.

The foundation geometry is assumed to comprise of a circular base with diameter of 35m and an upper conical section as described in (Smith, et al., 2015), see Figure 3-1 in section 3 . The seabed is assumed to be comprised of as coarse SAND to gravelly SAND sediments with a constant-volume friction angle (ϕ_{cv}) of 35 degrees.

Current design codes (e.g. DNV-J101 (pre-2014) ST-0126 / Eurocodes etc.) use a partial factor approach where partial factors are applied to actions (loads), materials and resistance to achieve the target safety level for the structure. For the purpose of this example and to allow better understanding of the sensitivity of results to different input parameters, an overall Factor of Safety (FoS) approach has been adopted. To this end the characteristic load/moment (S_k) and characteristic resistance (R_k) are calculated for different ultimate limit state checks (e.g. bearing and sliding) and the associated Factor of Safety (FoS) is calculated as follows:

$$FoS = \frac{S_k}{R_k} \qquad \text{Equation 5-1}$$

$$\text{Utilisation} = \frac{\text{Available FoS}}{\text{minimum FoS required}} \qquad \text{Equation 5-2}$$

For the purpose of comparison, the FoS values are expressed as utilisation calculated as the available FOS divided by minimum required FoS for each respective design check (i.e. bearing, sliding and overturning). It should be noted that for a concept/detailed design scenario consideration shall be taken for application appropriate load and resistance factors according to

recommendations in DNV-J101 (pre-2014) ST-01226. The minimum FoS values are taken from API's Recommended Practice for working on offshore platforms (2007). Overturning (1.5), bearing (2.0) and sliding checks (2.0) as set out in Table 3-7.

The bearing capacity calculation is performed based on recommendations from (DNV-GL, 2014) suggested a comprehensive method for bearing capacity which took into account the effects of shape and depth of the foundation as well as the inclination of the load applied.

The sliding check is performed based on recommendations in (DNV-GL, 2014) as a baseline case, and then further improved based on the proposed approach in thesis as discussed in Section 2.1. Figure 5-1 shows the available factor of safety for different ballast weights based on requirements for bearing, sliding and overturning for the pre-2014 method and Figure 5-2 show the refined approach.

5.2 Results

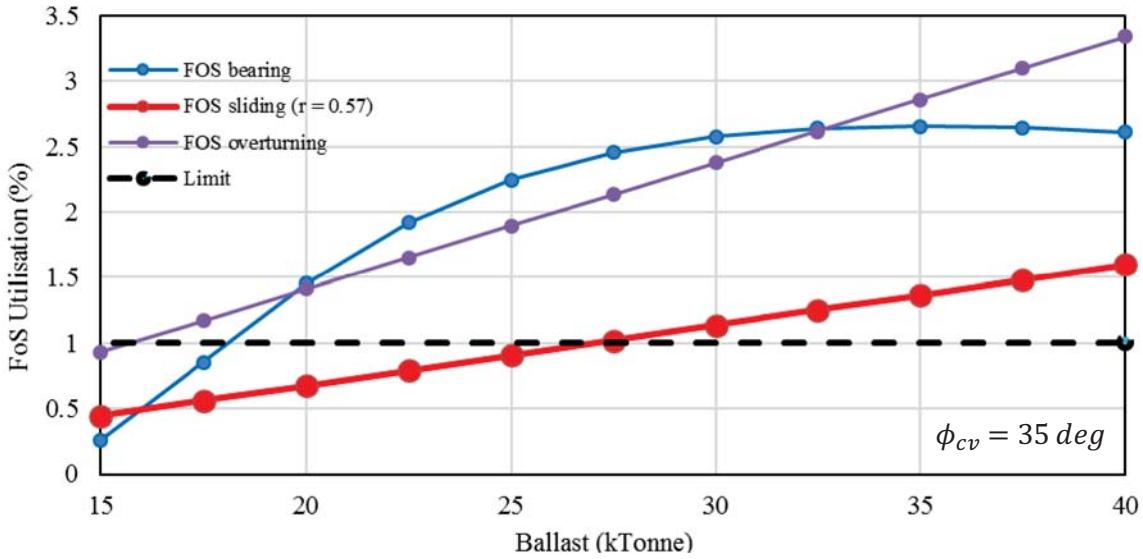

Figure 5-1: Variation in FOS with ballast weight (as utilisation of minimum required FOS) based on requirements for overturning, bearing and sliding (pre-2014 DNV-J101 method).

It can be observed in Figure 5-1 that the minimum required ballast weight based on the bearing, sliding, and overturning checks are calculated with the sliding requirement governing the design for ballast weight. This pre-2014 calculation applies a roughness coefficient (r) of 0.57 based the method in equation 3-6. The background information, design basis and calculations for the results in Figure 5-1 can be found in Section 3.1. It can also be observed that at approximately 35kTonne the FoS decreases. There is an FoS utilisation decrease between 35 and 40kTonne, from 5.31 to 5.22. This is showing that this fixed based-bottom is tending towards bearing failure as weight increase.

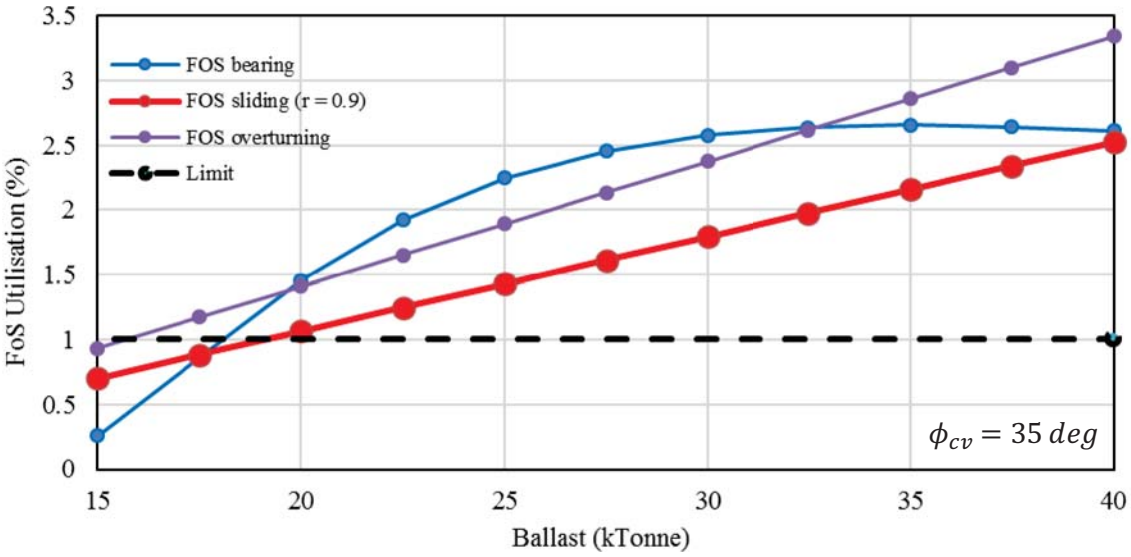

Figure 5-2: Variation in FOS with ballast weight (as utilisation of minimum required FOS) based on requirements for overturning, bearing and sliding (method suggested in this MAI project)

An alternative calculation is provided in Figure 5-2 where the sliding capacity is determined based on the refined approach presented in this thesis, where all values are identical to the pre-2014 calculation in Figure 5-1 but the roughness coefficient (r) is 0.9 based on the results from the lab results in Section 4. The background information, design basis and calculations for the results in Figure 5-2 can be found in Section 3.1. It is observed that the minimum required ballast weight using this approach is reduced from 26.993 kTonne to 19.081 kTonne, which represents a 29% saving in the ballast material required. This would have benefits in terms of associated procurement, staging and installation costs.

Influence of seabed type

In order to assess the influence of seabed type, the analysis was subsequently repeated to include a range of seabed conditions from fine grained SAND to sandy GRAVEL with constant-volume friction angle between 35 and 50 deg. Figure 5-3 shows the required ballast weight based on requirements for overturning stability (red dashed line), bearing capacity (blue dashed line), sliding capacity using DNV-J101, pre-2014 approach (green dashed line), and sliding capacity using approach proposed in this study (black dashed line).

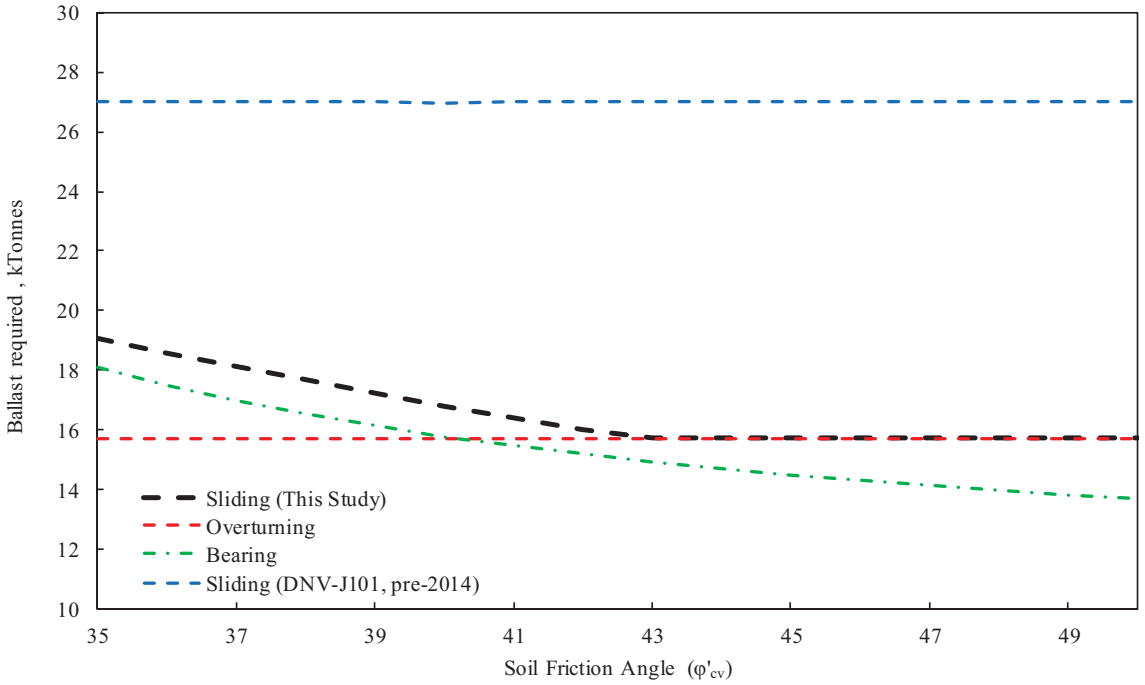

Figure 5-3: Comparison of the required ballast weight based on overturning, bearing, and sliding criteria using industry standard DNV-J101 (pre-2014) approach and also the approach proposed in this study

It can be observed that the sliding capacity calculated using old DNV-J101 (pre-2014) approach governs the design of ballast weight for all friction angles considered. It is also observed that the adoption of approach proposed in this study can significantly reduce the required ballast for the range of friction angles considered. The revised sliding capacity still governs the ballast requirement in this example for friction angles less than 43 deg. However, for higher friction angles, the overturning criterion dominates and no further reduction in ballast as a result of adoption of refined sliding formulation can be realised.

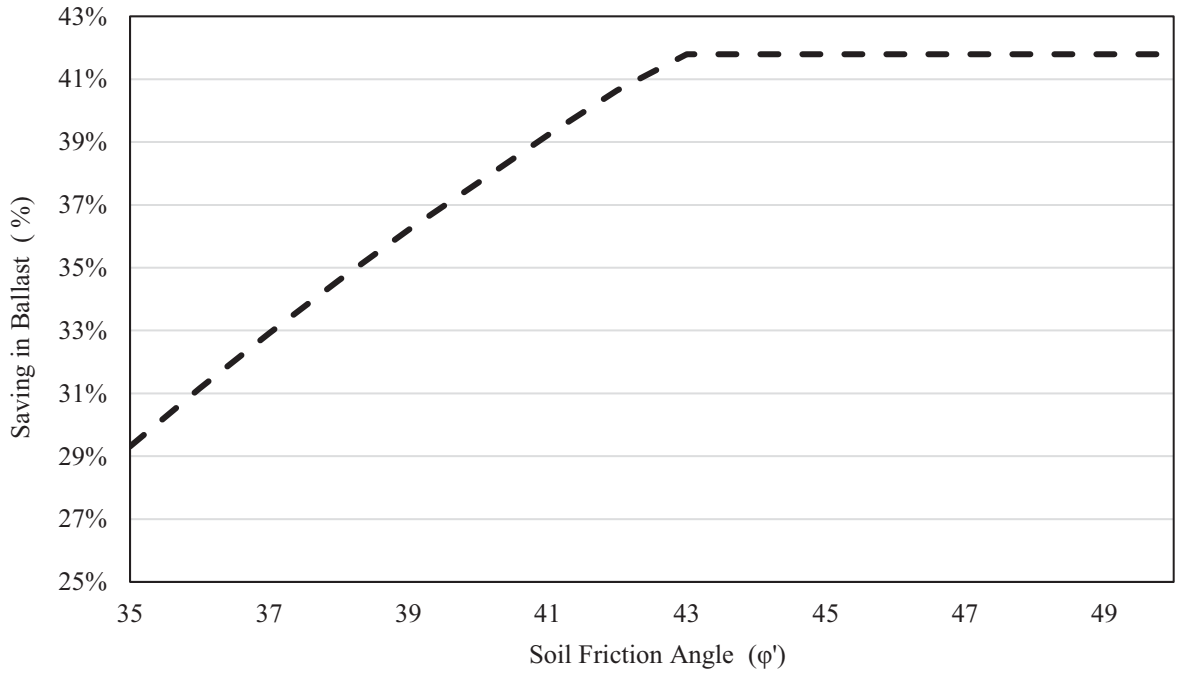

Figure 5-4: Ballast saved due to adoption of refined sliding capacity calculation for ϕ_cv=35-50 deg

Figure 5-4 shows where savings in ballast based on Figure 5-3 which compares the pre-2014 method of calculating *(r*) to the refined method in this thesis. It is shown that the ballast savings can vary between 29% and 42% can be achieved depending on the friction angles considered. It should be noted that most savings in this worked example are realised at higher friction angles.

5.3 Summary

This section carried out worked examples demonstrating how the proposed refined approach of calculating (r) improves on the pre-2014 method. It demonstrates cost saving (in the form of a reduction in ballast weigh requirements) that can be achieved by examining the sliding resistance, bearing capacity and overturning stability at preliminary design stage. The results from the laboratory work and similar geometry/parameters to the 3DFE analysis were used.

It compared the sliding capacity criterion of the pre-2014 method (r = 0.57) and for the proposed approach (r = 0.9) against ballast ranging from 15kT and 40kT. It was observed that the minimum required ballast weight using the refined approach is reduces from 26.993 kTonne to 19.081 kTonne, which represents a 29% saving in the ballast material and associated procurement, staging and installation costs.

In order to assess the influence of seabed type, the analysis was subsequently repeated to include a range of seabed conditions from fine grained SAND to sandy GRAVEL with constant-volume friction angle between 35 and 50 deg. It is shown that significant ballast savings can be achieved,

vary between 29% and 42% can be achieved depending on the friction angles considered. It should be noted that most savings in this example are realised at higher friction angles. The revised sliding capacity still governs the ballast requirement in this example for friction angles less than 43 deg. However, for higher friction angles, the overturning criterion dominates and no further reduction in ballast as a result of adoption of refined sliding formulation can be realised.

6 Finite Element Analysis

Finite Element Analysis was carried out in Plaxis 3D which assessed the foundation capacity relative to applied loads and then verified through a safety analysis. It used a similar design basis as the worked example in Section 5. base diameter, loading etc) and soil parameters from the commissioned lab testing, the definition of roughness coefficient (r) understood by Plaxis is the same as that calculated in the laboratory tests in Section 4. This case study compared the performance of the serrated GBF at the lower, middle and upper end of the ballast range and produce lateral displacement (sliding) and vertical displacement (settlement) with associated FoS. Also, the differential settlement (tilt) was calculated for the three ballast units assessed.

In order to perform a numerical analysis in Plaxis 3D, firstly, a model of the body of soil, structural forces/applied loads and interfaces was built. Realistic modelling of the soil layer, structural shape and characteristics as well as the assumptions used for defining the soil-structure interaction are of utmost importance in acquiring reliable results.

A case study was conducted for a GBF (serrated base) at the lower, middle and upper end of the ballasts range examined in Section 6; 20 kT, 30kT and 40kT respectively. Phased construction was employed where increasing increments of 10% of the loading associated with each ballast quantity were added. This was done by applying a percentage of the horizontal load (F_y), vertical load(F_z) and moment (M_x) to the base plate. Table 6-1 gives an example for 10% and 20% of total loading for 20 kTonne.

Table 6-1: Example of phased construction methodology for the 20kT ballast case

Loading	F_y [kN]	F_z [kN]	M_x [kNm]
Total loading for 20kT ballast (100%)	42500	-143900	118800
10% of total	4250	-14390	11880
20% of total	8500	-28780	23760

Results for total displacement |U|, vertical displacement (settlement) $|U_z|$and lateral displacement $|U_y|$ (sliding) values for the serrated based GBF were outputted against the applied phase loading. Next, each of these results were presented against a FoS. Finally, the differential settlement was calculated for the three cases.

Lateral and vertical displacements were measured from the model centre point (0,0,0). Differential settlement was calculated by comparing the relative difference in vertical displacement of two points on the edge of the baseplate node 17 and node 2 are along the y-y axis as illustrated in Figure 6-1 (see also Table 0-2 in Appendix A).

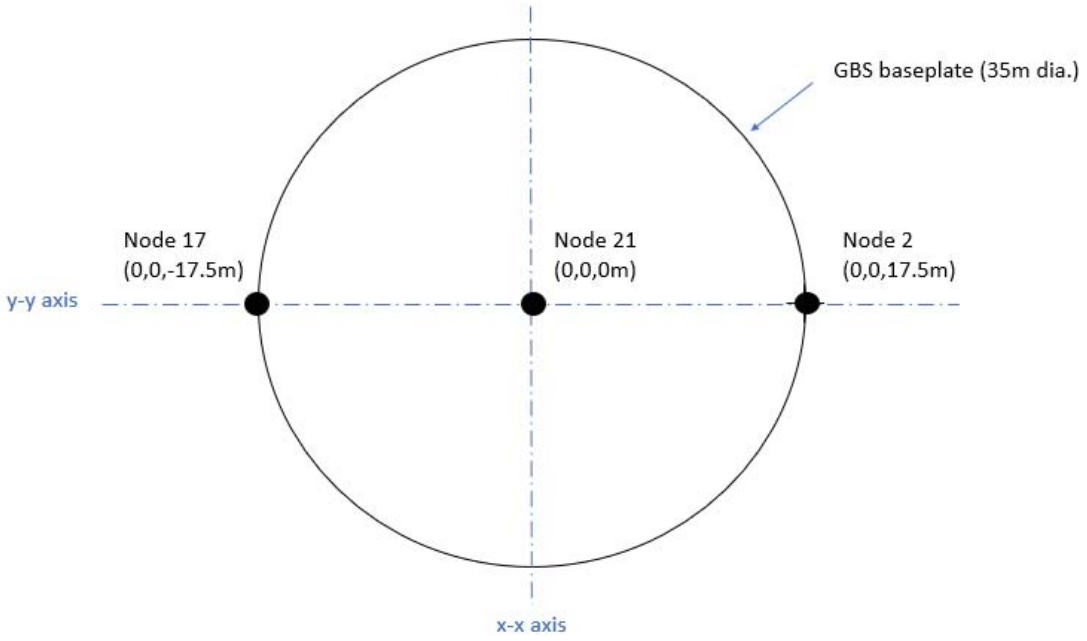

Figure 6-1: Location on baseplate to measure settlement, vertical and horizontal displacements

A step by step description of the construction of the 3D FE Model is provided in Appendix 0.

6.1 Results - Finite Element Analysis

The results of the Plaxis 3D are presented in this section. Vertical and lateral displacement and associated FoS results of serrated GBFs at the lower, middle and upper end of the ballast range are shown. Differential settlement (tilt) of the GBF base for the same ballast ranges is also presented.

6.1.1 Vertical Displacement

The vertical displacement of the serrated base plate when loads associated with 20kT, 30kT and 40kT ballast are applied is shown in Figure 6-2. It can be seen that displacement values rise steadily for all threes ballast units from 10% to the total ballast amount (100%). All phases passed the Plaxis 3D analysis meaning that the bearing capacity and sliding resistance capable of supporting the loads up to 40kT. It can be seen, as expected, that the rate of increase is steeper the greater the total ballast; the average phase increase in vertical displacement for 20kt is 0.005m, 30kT is 0.010m and 0.014m for 40kT. It also can be seen that the total displacement

(100% ballast) increases, as expected, the greater the ballast; vertical displacement ranged from 0.050m for 20kT, 0.92m for 30kT and 0.135m for 40kT. Figure 6-2 is shows the vertical displacements |Uz| for the lower, middle and upper ballast range.

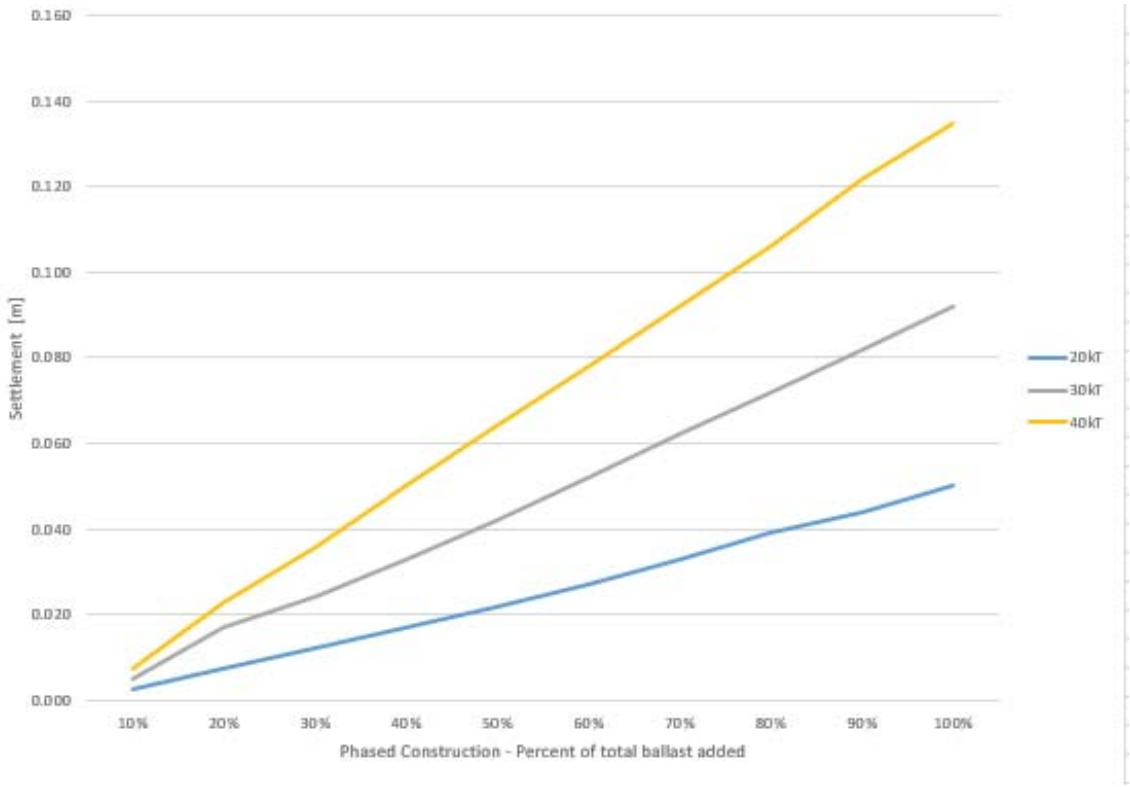

Figure 6-2: Graph of vertical displacements $|U_z|$ for the lower, middle and upper ballast range

Curves were generated in Plaxis 3D that plotted Vertical displacements $|U_z|$ for against a factor of safety (∑Msf). Figure 6-3 shows a comparison of FoS achieved for the three cases studied taken at the centre point of the model (see node 21 in Figure 6-1). It can be seen that the resulting global safety factor in all cases reached >2, which indicated a low susceptibility to foundation bearing failure.

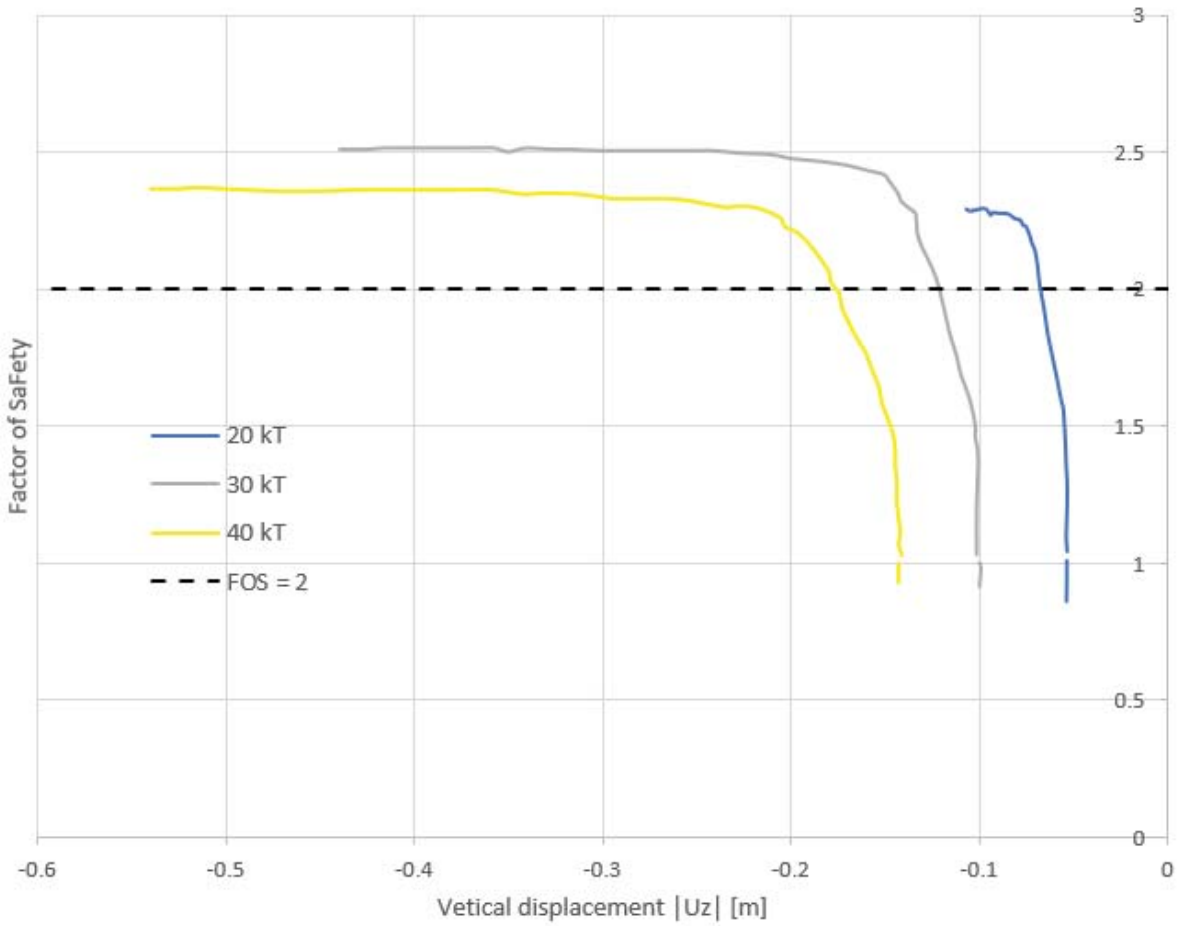

Figure 6-3: Comparison of vertical FoS of 20kT, 30kT and 40kT loadings

6.1.2 Lateral Displacement

The Plaxis outputted lateral displacements $|U_y|$ for 20kT, 30kT and 40kT loading was analysed. It can be seen that there is only a very minor difference in the sliding ballast weights assessed with only 0.001m difference in movement between 20kT, 30kT and 40kT when the model is fully loaded. Figure 6-4 shows that movement is negligible at up to approx. 35% of total load.

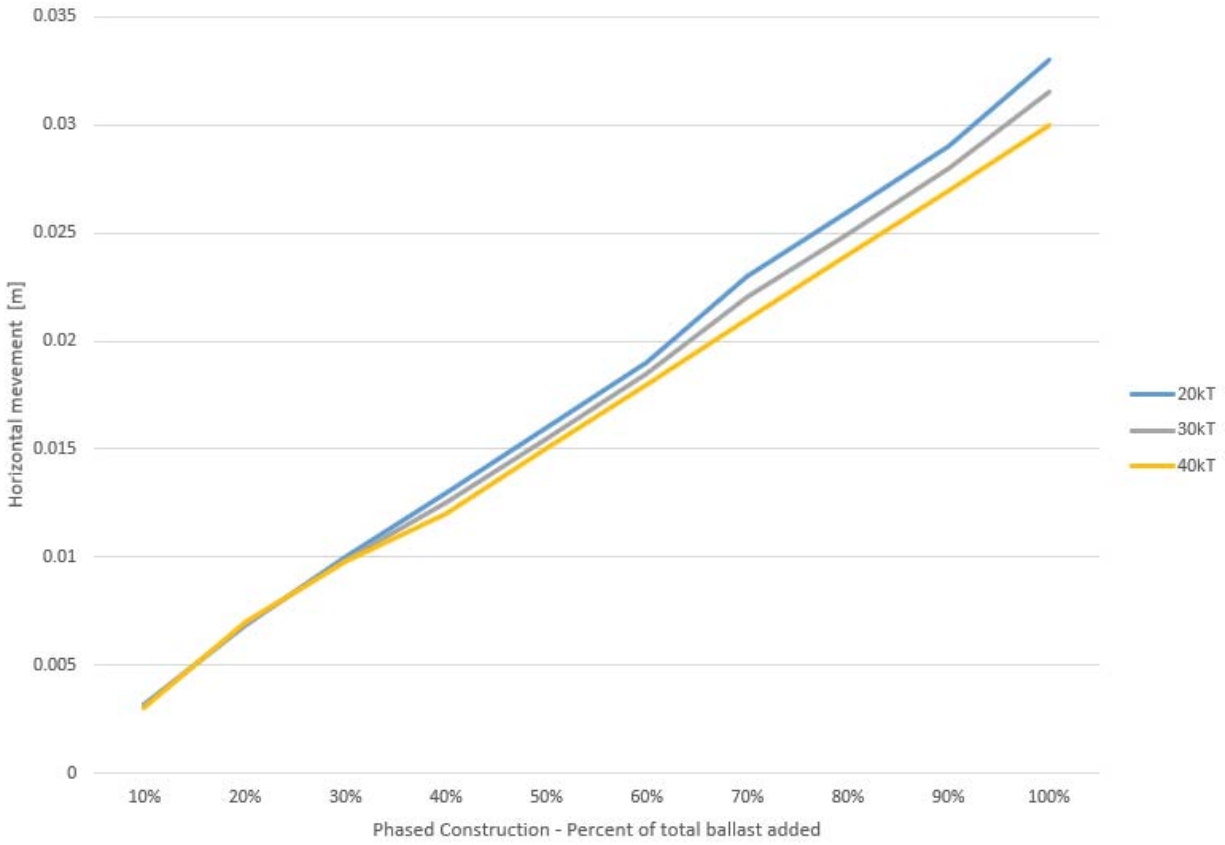

Figure 6-4: Horizontal displacement for phased construction of 20kT, 30kT and 40kT loading

Curves were generated in Plaxis 3D that plotted lateral displacements | U_y | against a factor of safety (∑Msf). Figure 6-5 shows a comparison of FoS achieved for the three cases studied. In all cases the minimum global factor of safety against sliding was > 2, which is considered sufficient.

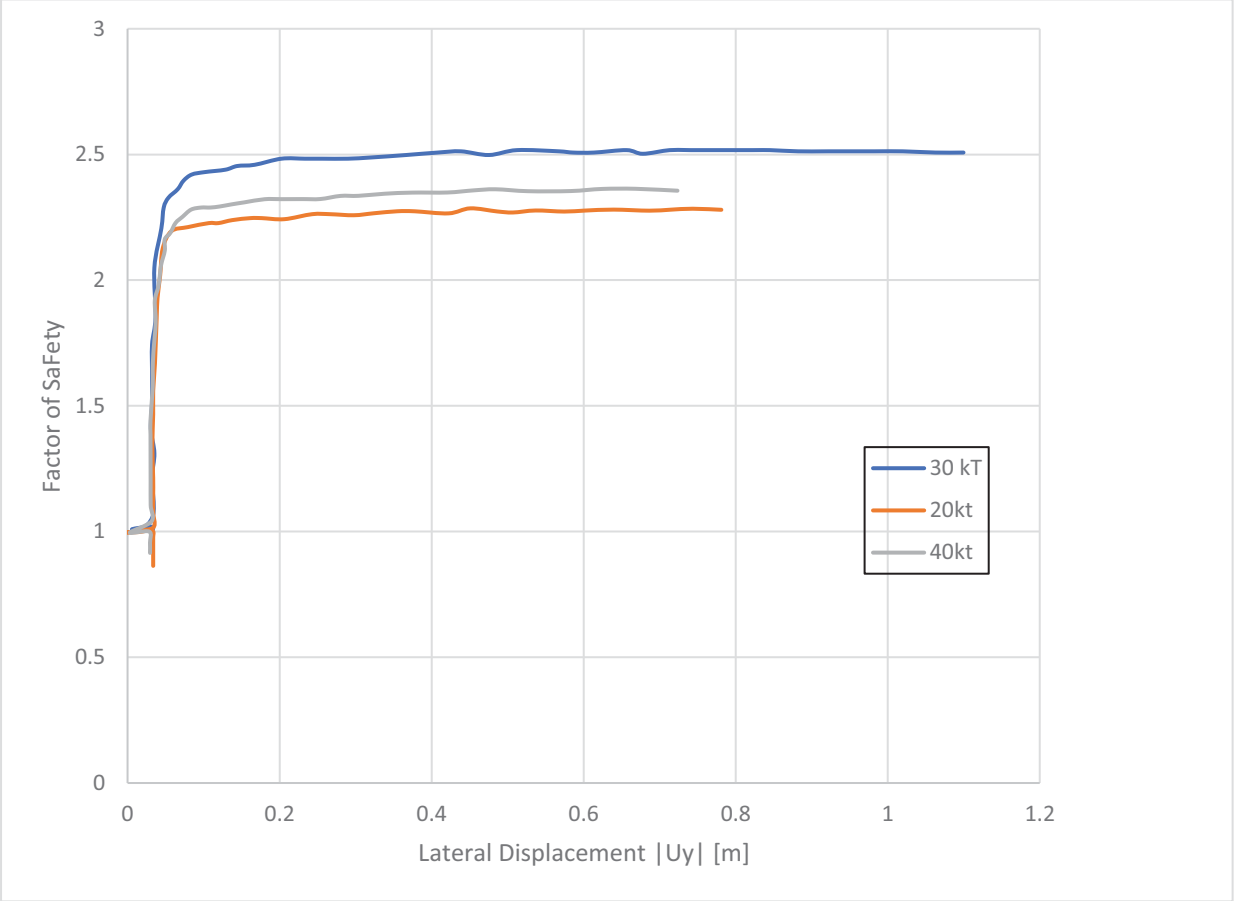

Figure 6-5: FoS Comparison of lateral displacement FoS of 20kT, 30kT and 40kT loadings

6.1.3 Differential Settlement

The tilt was calculated by analysing the vertical displacement in the safety phase by comparing vertical placement of nodes 2 and 17 (see Figure 6-1 and Table 0-2). It was assumed that the system rotates as a rigid body. Table 6-2 shows the results of the GBF differential settlement.

Table 6-2: Results of GBF differential settlement

Ballast Unit	Maximum Vertical Displacement - Node 17 [mm]	Minimum Vertical displacement - Node 2 [mm]	Relative Difference [mm]	Tilt [°]
20kT	-315	-130	185	0.087
30kT	-626	-250	376	0.286
40kT	-769	-307	462	-4.70

The result show that the loading of 20kT is within the tilt tolerance of 0.25°, 30 kT is marginally outside while 40kT is significantly out of tolerance.

7 Discussion

The central question of this thesis is to explore if efficiencies can be achieved in the design of gravity-based foundation (GBF) for offshore wind turbines and if a reduction in quantity of material required to ballast the structure is possible. It did this through a refinement to the current method of calculating sliding resistance and demonstrates this through a series of analyses that offer solutions to gaps in knowledge on this topic.

After the proposed refined approach to calculate the roughness coefficient (*r*) is put forward in Section 2.1 three separate exercise were carried out to expand upon it. Laboratory testing (commissioned work) that provided data to produce interpretations of friction and interface friction angles, ballast material requirement that compared the pre-2014 DNV method of quantifying ballast quantities to the refined method and a FEA analysis that quantified vertical and lateral displacements for a serrated base. The lab work provided roughness values (*r*) for the analytical and the FE studies.

Section 2.1 provides a background to the design codes and the development of the methods used to calculate sliding resistance. To help provide clarity to the industry an alternative was sought into how the roughness coefficient (r) is calculated; this thesis suggests an alternative approach to try fill this gap in knowledge in GBFs design. The tan of the interface friction angle ($\tan\delta$) divided by the tan of the soils internal friction angle ($\tan\varphi'$) as outlined in equation 2-8 is proposed as a formula to calculate r. By applying this formula to lab. results a more accurate estimate of r was calculated for the range of soils and interface type tested.

The commissioned laboratory testing provided good raw geotechnical data to aid this thesis. It produced similar results for gradings 1-3 to Dunne's testing (2019) and added in a fourth grading (fine sand from Blessington) at the request of the author of this thesis which Doherty et al. suggests has similar characteristic to specific to Irish Sea offshore sites (Doherty, et al., 2012). The roughness coefficients (*r*) calculated from the results are a vital piece of data for the refined formula which permitted completion of the ballast calculations (Section 5) and Plaxis modelling (Section 6) .The results provide new light on the variation of friction angles for soil on soil, serrated and smooth tests was large for coarse soil e.g. they ranged from 30 to 53 for coarse grain soils (G3) whereas the was less variation for Blessington Sand (G4).

Another potential use of the lab. results and possible additional study could be to calculate API sliding resistance (API method) outlined section 2.1. The lab results produced a range of soils

internal friction angles that could be applied to equation 2-2. This would allow a direct comparison of the API and DNV methods.

A ballast requirement analysis was carried out to demonstrate to industry how the refined sliding resistance calculation can lead to greater efficiencies in GBF design. The analysis showed how a 29% saving in ballast can be achieved; it was observed that the minimum required ballast weight using this approach is reduced from 26.993 kTonne to 19.081 kTonne, a saving of almost 8 kTonne. It also provides likely savings in ballast required for a range of seabed conditions (fine grained SAND to sandy GRAVEL). It concludes sliding capacity still governs design for friction angles below 43°; above this value overturning is the governing factor and no ballast savings can be achieved. This give developers a clear template to base early stage design and can be adapted to other offshore renewables sectors i.e. tidal and wave employing a similar foundation type.

Analysis in Plaxis 3D shows that with increased loading the vertical displacement increases; a 20 kTonne results in a 50mm, 30 kTonne equates to 92mm and 40 kTonne results in a 104mm within the permitted FoS, thus proving that the bearing capacity is sufficient in Blessington Sand to support the fully ballasted GBF. While some lateral displacement took place (average 31.5mm), it was insensitive to the ballast quantity tested. This was expected for a structure of such weight and vertical loading.

Due to the large loads being applied in the vertical direction the small saw-tooth serration (70mm deep in Demogravi3 project and 15mm in lab testing) offered certain amount of sliding resistance. Perhaps further testing on a courser material (e.g. grading 3 in the lab section has an r -value of 0.58) could show a reduction in sliding resistance. A serrated base interface cannot be considered in the same category as piles or skirting which penetrate meters into the seabed. In the analysis carried out by Attari (2016) where piles were compared to a flat base (without piles) there was significant decrease in lateral movement with piles.

Tilt was checked at the end of the FEA section. It showed that only the differential settlement associated with the 20 kTonne ballasted GBF (ΔS = 185 mm) was within the tilt tolerance of 0.25°, 30 kTonne was just outside tolerance and 40 k Tonne would mean failure with a tilt of 4.7°. The installing a flat bed of gravel in sufficient quantities help reduce tilt of these last two cases would be required, this has been the procedure in most installations to date.

It was the author's intention to study a soil typical to Irish sea conditions, hence, Blessington Sand (fine SAND) was added to the lab experiments (grading 4) which provides the roughness parameter (*r*) used in in Plaxis; the ground model was designed accordingly with a friction angle

of 35° assigned to the ground model based on the (Igoe & Gavin, 2019); however, the laboratory testing produced a lower friction angle (average of 30.5°) for the serrated base. The Plaxis results may not have been as favourable if this lower value were used.

The water depth (45m) selected was deeper than any installation to date and is very much looking to the future with the trend set to continue into deeper waters. The diameter (35m) was used for both analytical analysis and the FEA analysis and should be considered general; in practice, in early stage design the diameter would be varied to meet bearing, sliding and overturning to fall within the required FoS.

New understanding to the calculation of sliding and bearing capacities have been developed in this thesis and can be of use to the offshore sector and all aspects of this these helps to link the gap in the interpretation. However, the Plaxis 3D analysis could have looked at a wider range of ballasts and a wider range to soils (friction angles of 30 to 50°) and an expansion of this economic savings showing estimates for financial savings installation time, staging etc. is further work that can be done.

In conclusion, the thesis achieved its objectives as stated in Section 2.4. This discussion outlined why the research undertaken in this thesis is relevant, consolidated the findings and allowed for in-depth comparisons between all of the tests. It highlights gaps in current and past design codes, proposes refined approach and proceeds to expands on methods to obtain the roughness coefficient (*r*), apply, test and prove its validity. This study was carried out specifically for offshore wind (using a soon to be standard turbine size of 10MW). However, a reduction in ballast requirements can be applied to other offshore renewables sectors e.g. foundations for tidal devices.

During detailed design, a project must consider how the specific site characteristics affect the behaviour of the wind turbine and its support structure. Though the sliding capacity is considered an ultimate limit state, the load response behaviour of the interface between the foundation and the soil should also be considered. The results from the laboratory testing, may be considered during the assessment of the foundation's load response behaviour in terms of both frequency assessment and the foundation response as modelled during the analysis of the turbine.

8 Conclusion

Offshore wind energy production is set to expand globally into the future. As installations extend into different seabed conditions and deeper waters all foundation types will find their niche. The use of GBFs, although only 3.3% of the current installed fleet is due increase to 8.4% in the coming years.

The central question of this thesis was to explore if efficiencies can be achieved in the design of gravity-based foundation (GBF) for offshore wind turbines and if a reduction in quantity of material required to ballast the structure is possible. It did this through a refinement to the current method of calculating sliding resistance and demonstrates this through a series of analyses that offer solutions to gaps in knowledge on this topic.

The work contained herein have fulfilled the objectives of the thesis, which were to:

- Develop an equation based on previous studies to estimate the roughness coefficient (*r*).
- Analyse and interpret laboratory experimental results (commissioned work in Section 4) to establish the roughness coefficients (using equation proposed in Section 2.1) for flat-based and serrated bottoms for range of typical offshore seabed types;
- Determine the reduction in ballast material required from adoption of more refined approach for calculation of sliding resistance (compared to pre-2014 DNV method) based on experimental testing (analytical calculations in Section 5);
- Carry out stability checks by establishing vertical and lateral displacements along with differential settlement for the GBF in Blessington Soil using a 3DFE software (Section 6).

This thesis commenced with a comprehensive background into use of GBF in the offshore wind industry. It sets out the design challenges facing developers that choose a GBF option and outlines some gaps in the designs codes where there is scope to become more efficient i.e. save in material usage.

The proposed refined method to calculate the roughness coefficient (*r*) is put forward and three separate exercise were carried out to build on this approach; lab experimentation, hand calculations and FE analysis.

Laboratory testing (commissioned work) that provided data to produce interpretations of friction and interface friction angles, analytical analysis that compared the pre-2014 DNV method of quantifying ballast quantities to the refined method suggested in this thesis. The variation of friction angles for soil on soil, serrated and smooth tests was large for coarse soil e.g. they ranged from 30 to 53 for coarse grain soils (G3) whereas the was less variation for Blessington Sand (G4).

It was observed that the sliding capacity calculated using old DNV-J101 (pre-2014) approach governs the design of ballast weight for all friction angles considered. It is also observed that the adoption of approach proposed in this study can significantly reduce the required ballast for the range of friction angles considered. The hand calculations showed that the minimum required ballast weight using this approach is reduced from 26.993 kTonne to 19.081 kTonne, which represents a 29% saving in the ballast material and associated procurement, staging and installation costs. The revised sliding capacity still governs the ballast requirement in this example for friction angles less than 43 deg. However, for higher friction angles, the overturning criterion dominates and no further reduction in ballast as a result of adoption of refined sliding formulation can be realised.

Finally, the FE analysis produced vertical and lateral displacements for the GBF assessed in Section 6) along with differential settlement for a GBF in Blessington Sand. Analysis in Plaxis 3D shows that with increased loading the vertical displacement increases; a 20kTonne results in a 50mm, 30kTonne equates to 92mm and 40kTonne results in a 104mm within the permitted FoS, thus proving that the bearing capacity is sufficient in Blessington Sand to support the fully ballasted GBF. While some lateral displacement took place (average 31.5mm), it was insensitive to the ballast quantity tested. This was expected for a structure of such weight and vertical loading.

All elements of this thesis combined helped to demonstrate that through a refinement of the design approach to sliding resistance, reliable geotechnical data relating to soil and interface friction angles, early stage estimates of ballast requirement and application of advanced FE analysis a significant savings can be achieved in offshore wind turbine installation employing a GBFs.

References

4COffshore, 2018. *4C offshore.* [Online] Available at: https://www.4coffshore.com/gravitybasedfoundations [Accessed 10 October 2018].

Ahmadi, M. & Ghazavi, M., 2012. *Effect of Skirt Geometry Variation On Uplift Capacity of Skirted Foundation,* Rhodes, Greece: Proceedings of the International Offshore and Polar Engineering Conference.

API, 2007. *Recommended Practice for Planning, Designing and Constructing Fixed Offshore Platforms—Working Stress Design,* Washington: American Petroleum Institute.

API, 2011. *API-RP-2GEO Geotechnical and Foundation Design Considerations,* Washington: American Petroleum Institute.

Attari, A. et al., 2014. *LEANWIND Deliverable D3.1 - Novel Vessels and Equipment,* Brussels: European Union's Seventh Programme for research, technological development and demonstration .

Attari, Y., 2016. *Performance Testing of a Novel Gravity Base Foundation for Offshore Wind,* Dublin: University College Dublin.

Bak, C. et al., 2013. *DTU Wind Energy Report - Design and performance of a 10 MW wind turbine* , Roskilde, Denmark: DTU Wind Energy.

BAM, 2017. *https://www.bam.com.* [Online] Available at: https://www.bam.com/en/press/press-releases/2017/8/blyth-offshore-demontrator-wind-farm-project-first-gravity-base [Accessed 4 July 2019].

Bolton, M. D., 1986. The strength and dilatancy of sands. *Géotechnique* , 10 January, p. 65–78.

Bond, A. & Harris, A., 2009. *Decoding Eurocode (Part 2).* London & New York: Taylor & Francis.

Brinkgreve, R., Engin, E. & Engin, H., 2010. *Validation of empirical formulas to derive model parameters for sands.* Delft, CRC Press.

de Temiño, A. I. R., 2013. *Gravity Based Foundations for Offshore Windfarms,* Santander, Spain: University of Cantabria.

De vries, W., 2011. *Support Structure Concepts for Deep Water Sites, WP4.2: offshore foundations and support structures,* Brussels: EC Upwind Project.

DNV-GL, 2013. *DNV-OS-J101 Design of Offshore Wind Turbine Structures,* Arnhem, The Netherlands: Det Norske Veritas - Germanischer Lloyd.

DNV-GL, 2014. *DNV-OS-J101 Design of Offshore Wind Turbine Structures.* Arnhem, The Netherlands, Det Norske Veritas - Germanischer Lloyd.

DNV-GL, 2017. *DNVGL-RP-C212 Offshore soil mechanics and geotechnical engineering,* Arnhem, The Netherlands: Det Norske Veritas - Germanischer Lloyd.

DNV-GL, 2018. *DNVGL-ST-0126 Support structures for wind turbines,* Arnhem, The Netherlands: Det Norske Veritas - Germanischer Lloyd.

DOE, U.S, 2018. *2018 Offshore Wind Technologies Market Report,* Oak Ridge, TN: U.S Department of Energy.

Doherty, P. et al., 2012. *Soil Properties at the UCD Geotechnical Research Site at Blessington.* Dublin, University College Dublin.

Dunne, J., 2019. *Sliding Friction of Gravity Base Foundations for Tidal Energy Devices,* Dublin: Trinity College Dublin.

Elhakim, A. F., 2005. *Evaluation of Shallow Foundation Displacements Using Soil Small-Strain Stiffness,* Atlanta: Georgia Institute of Technology.

Esteban, M. et al., 2015. Gravity based support structures for offshore wind turbine generators: Review of the installation process. Volume 110, p. 281–291. .

Gavin, K. G. & Lehane, B., 2005. Base Load – Displacement Response of Piles in Sand. *Canadian Geotechnical Journal*, 17 October, p. 1053–63.

Gavin, K. G. & O'Kelly, B. C., 2007. Effect of Friction Fatigue on Pile Capacity in Dense Sand. *Journal of Geotechnical and Geoenvironmental Engineering,* 133(1), pp. 63 - 71.

Gourvenec, S. & Barnett, S., 2011. Undrained failure envelope for skirted foundations under general loading. *Geotechnique,* 61(3), pp. 263-270.

Herold, A. & von Wolffersdorff, P. A., 2009. The Use of Hardening Soil Model with Small-Strain Stiffness for Serviceability Limit State Analyses of GRE Structures. *GeoAfrica*, 2 May, pp. 1-8.

Igoe, D., 2018. *CE7S06_Offshore Geotechnical Engineering module.* Dublin: Dept. Civil Engineering, Trinity College Dublin .

Igoe, D. & Gavin, K., 2019. Characterization of the Blessington sand geotechnical test site. *AIMS Geoscience*, 15 May, Volume 2, p. 145–162.

Igoe, D., Gavin, K. & O Kelly, B. C., 2011. *Shaft Capacity of Open-Ended Piles in Sand,* October, 137(10), p. 903–13.

ISO, 2014. *ISO 19901-4 Petroleum and natural gas industries — Specific requirements for offshore structures — Part 4: Geotechnical and foundation design considerations,* Geneva: ISO.

Jalali, M. M. et al., 2012. Using Finite Element Method for Pile-Soil Interface (through PLAXIS and ANSYS). November, 3(10), p. 256–72.

Klijnstra, J., Zhang, X., van der putten, S. & Röckmann, C., 2017. *Technical Risks of Offshore Structures.* 1 ed. Wageningen: Springer.

Knappett, J. & Craig, R., 2012. *Craig's Soil Mechanics - 8th edition.* London: Taylor and Francis.

Lade, P., 2005. *Overview of Constitutive Models for Soils, in: Soil Constitutive Models.* Austin, Presented at the Geo-Frontiers Congress.

Malhotra, S., 2011. *Wind Turbines - Chapter 10: Selection, Design and Construction of Offshore Wind Turbine Foundations.* s.l.:IntechOpen.

Murray, J. J., Booton, M., Mak, L. M. & Sullivan, a. M., 1992. *Model Design and Testing of a Large Gravity-Base Offshore Structure,* St. John's, Newfoundland: Institute of Marine Dynamics.

Piere, K., 2009. Gravity Base Foundation for the Thornton Bank Offshore Wind Farm. *Terra et Aqua*, 1 June, pp. 20 - 29.

PLAXIS, 2019. *Plaxis Version - Materials Model Manual.* Exton, Pennsylvania: Bentley Systems.

Potvin, A. B., 1990. *Finite Element Analysis in Offshore Geotechnics - A Thirty-Year Retrospective.* Providence, RI, Exxon Production Research.

Prendergast, L., Hester, J., Gavin, K. & O'Sullivan, J., 2013. An Investigation of the Changes in the Natural Frequency of a Pile Affected by Scour. *Journal of Sound and Vibration,* 332(25), p. 6685–6702.

Randolph, M. & Gouvenec, S., 2011. *Offshore Geotechnical Engineering.* 1st ed. New York: Spon Press: Taylor and Francis Group.

Reyes, S. F. & Deene, D. K., 1966. *Elastic Rustic Analysis of Underground Openings by the Finite Element Method.* Lisbon, Proceedings of the 1st Congress of the International Society of Rock Mechanics, pp. 477-486.

Seatower, 2013. *http://seatower.com/technology/.* [Online] Available at: http://seatower.com [Accessed 5 September 2019].

Smith, J., Mickovski, S. B. & Hytiris, N., 2015. *Comparison of settlement calculation methods for the design of a gravity base foundation in deep water.* Glasgow, Glasgow Caledonian University.

Sturm, H., 2011. Geotechnical Performance of a Novel Gravity Base Type Shallow Foundation for Offshore Wind Turbines. *Geotechnik,* 34(2), p. 85–96.

The Carbon Trust, 2015. *Identifying the Key Barriers to Large Scale Commercialisaton of Gravity Based Structures(GBSs) in the Offshore Wind Industry,* London: The Carbon Trust.

Tistel, J. et al., 2015. *Gravity-Based Structure Foundation Design and Optimization Opportunities.* Kona, Hawaii, International Society of Offshore and Polar Engineers (ISOPE).

Tolooiyan & Gavin, K. a. A., 2011. *Modelling the Cone Penetration Test in Sand Using Cavity Expansion and Arbitrary Lagrangian Eulerian Finite Element Methods,* Dublin: Elsevier.

Velarde, J., 2016. *Design of Monopile Foundations to Support the DTU 10 MW Offshore Wind Turbine,* Delft: Delft University of Science and Technology.

WindEurope, 2019. *Wind Europe.* [Online] Available at: https://windeurope.org/about-wind/reports/wind-energy-in-europe-outlook-to-2020/#download [Accessed 10 October 2019].

Woodward, R. & Clough, R., 1967. *Application of the Finite Element Method in Geotechnical Engineering.* Vicksburg, Mississippi: U.S. Army Engineer Waterways Experiment Station, Corps of Engineers.

Zdravković, L. & Potts, D. M., 1999. *Finite Element Analysis in Geotechnical Engineering.* 1 ed. London: Thomas Telford.

Appendix A – Step by Step Construction of 3DFE Model

Definition of Project Dimensions

Modelling procedure in Plaxis 3D starts by defining the project dimensions, basic units, defining soil contours and general values such as specific weight of water. The footprint of the GBF base was assigned a 35m diameter. The rule of thumb is to create a soil model over two times the size of the base in order to capture the complete effect of the structure on the seabed. Due to the large ballast being assessed conservative project dimensions of 100m x 100m was selected. The FE analysis model was created using the half-space option in PLAXIS.

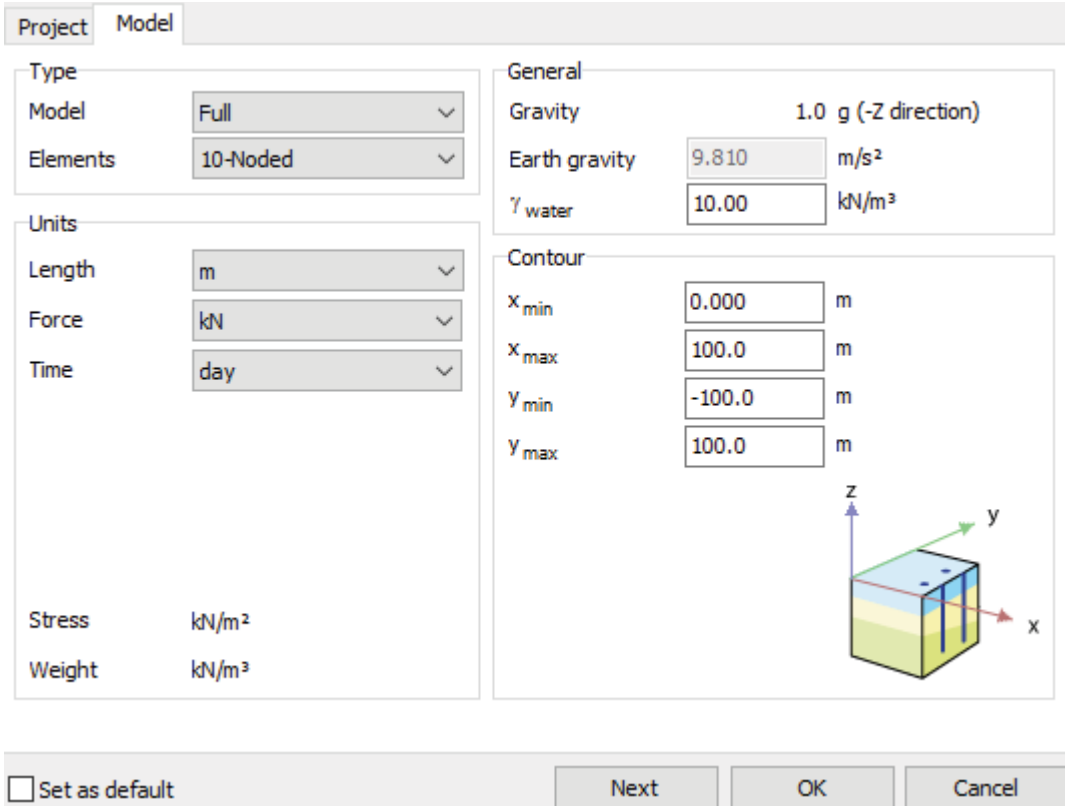

Figure 0-1: Definition of project dimensions

Specifying the Material Properties

After defining the soil boundaries, one or more boreholes are required to be characterised in order to define the various soil layers. The soil material was based on Blessington Sand applying HSsmall parameters for (see Table 3-8). Figure 0-1 illustrates the HSSmall parameters inputted into Plaxis.

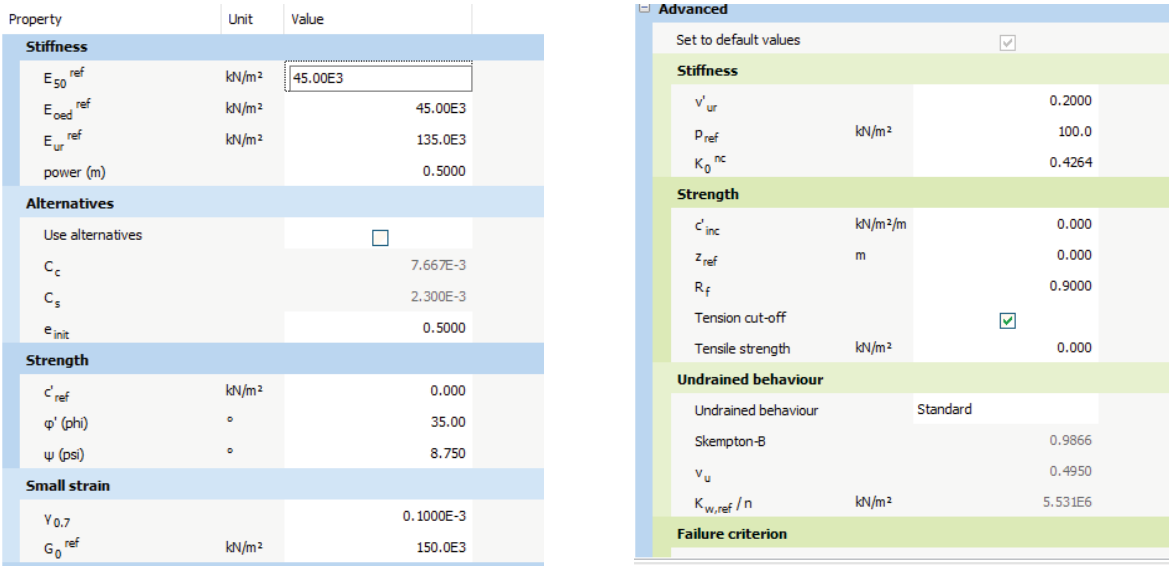

Figure 0-2: HSSmall parameters for Blessington Sand used in Plaxis

Creating the GBF Structure

To represent the GBFs a cylinder of 35m diameter was created and decomposed into a surface. In order to mimic a rigid GBF base the material created was assigned extremely high stiffness properties as outlined in Section 3.2.2. The value used was 20.00x10^9 kN/m^3 as shown in Figure 0-3. All loads were applied to the centre of the plate at the soil structure interface i.e. co-ordinate 0,0,0.

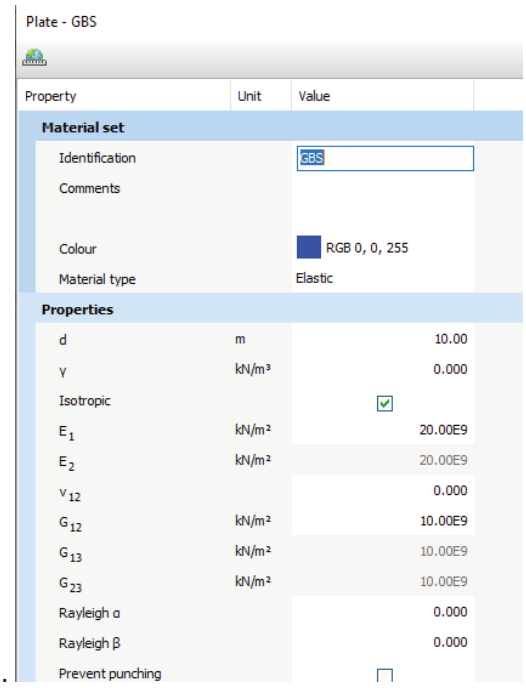

Figure 0-3: GBF plate properties

Creating an Interface to the Serrated Type Base

An Interfaces was set up to control the way the structure interacted with the soil. To mimic the behaviour of a serrated concrete interface a separate interface materials were created and assigned a roughness coefficient (r) of 0.9 (Figure 0-4 is a graphical representation),

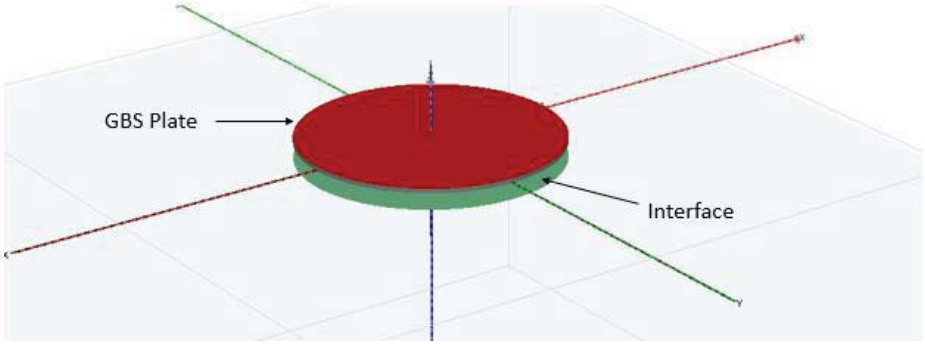

Figure 0-4: GBF Base plate and interface

Application of the Loads to the Model

Plaxis 3D offers a number of options when defining the calculation and loading type for deformation analysis. The initial phase was assigned a K0 procedure, phases 1 to 11 were assigned a plastic calculation type, while phase 12 was assigned a safety calculation type. The loading type applied was staged construction for the initial phase and phases 1 to 11 and incremental multiplier for phase 12. The sequence of the model followed the phasing outlined in Table A-1. The initial phase assesses the material set-up and calculates the initial stresses. This is the primary phase for every analysis where the soil layers are activated.

Table A-1: Construction phase parameters

Phase	Active Attribute	% of total ballast	Calculation Type	Loading Type
Initial Phase	Material Set-Up and Initial Stresses.	---	K0 Procedure	Staged Construction
Phase 1	Soil model & Interfaces	---	Plastic	Staged Construction
Phase 2	Soil model, Interfaces, loads	10% of total	Plastic	Staged Construction
Phase 3	Soil model, Interfaces, loads	20% of total	Plastic	Staged Construction
Phase 4	Soil model, Interfaces, loads	30% of total	Plastic	Staged Construction

Phase 5	Soil model, Interfaces, loads	40% of total	Plastic	Staged Construction
Phase 6	Soil model, Interfaces, loads	50% of total	Plastic	Staged Construction
Phase 7	Soil model, Interfaces, loads	60% of total	Plastic	Staged Construction
Phase 8	Soil model, Interfaces, loads	70% of total	Plastic	Staged Construction
Phase 9	Soil model, Interfaces, loads	80% of total	Plastic	Staged Construction
Phase 10	Soil model, Interfaces, loads	90% of total	Plastic	Staged Construction
Phase 11	Soil model, Interfaces, loads	100% of total	Plastic	Staged Construction
Phase 12	Safety Phase	Safety phase	Safety	Incremental Multiplier

Meshing

Once the soil, interfaces, material properties and the prescribed loading has been assigned the soil-structure system is meshed. Plaxis 3D meshes geometries into equilateral triangles. The sizes of these triangles are defined by the mesh coarseness for each individual surface or volume. It is refined in the vicinity of the structure but coarsened towards the boundary of the model. Figure 0-5 shows the mesh settings used.

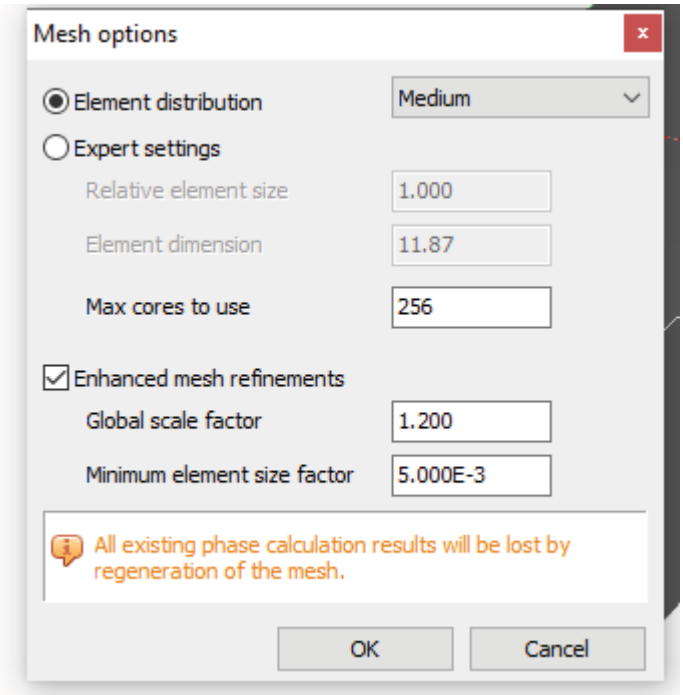

Figure 0-5: Mesh Settings

Nodes were added to the model as specific points to for ease of reading results at these important locations. Lateral and vertical displacements were measured from the model centre point (0,0,0). Differential settlement was calculated by comparing the relative difference in vertical displacement of node 17 and node 2 along the y-y axis as illustrated in Figure 6-1 and Table 0-2.

Table 0-2: Coordinates of nodes along the y-y axis used in FE analysis

	X (m)	Y (m)	Z (m)	Use in FE Analysis
Node 21	0.00	0.00	0.00	Lateral and vertical displacement values taken from this node
Node 17	0.00	-17.50	0.00	Differential settlement
Node 2	0.00	17.50	0.0	Differential settlement

Safety Analysis Phase

An additional phase was added to the model to assess safety. The loading combinations examined using Safety Analysis (SF) and the global safety factor for the foundation was calculated. The safety calculation computes global safety factors by reducing the shear strength parameters (tan ϕ and c) of the soil, along with the tensile strength, until failure of the structure occurs. The reduction in strength parameters was performed according to:

$$\sum Msf = \frac{\tan\varphi\ input}{\tan\varphi\ reduced} = \frac{\mathrm{C}\ input}{\mathrm{C}\ reduced}$$ Equation 6-1

Where $\sum Msf$ corresponds to the global safety factor. Figure 0-6 shows the safety calculations parameter used in Plaxis.

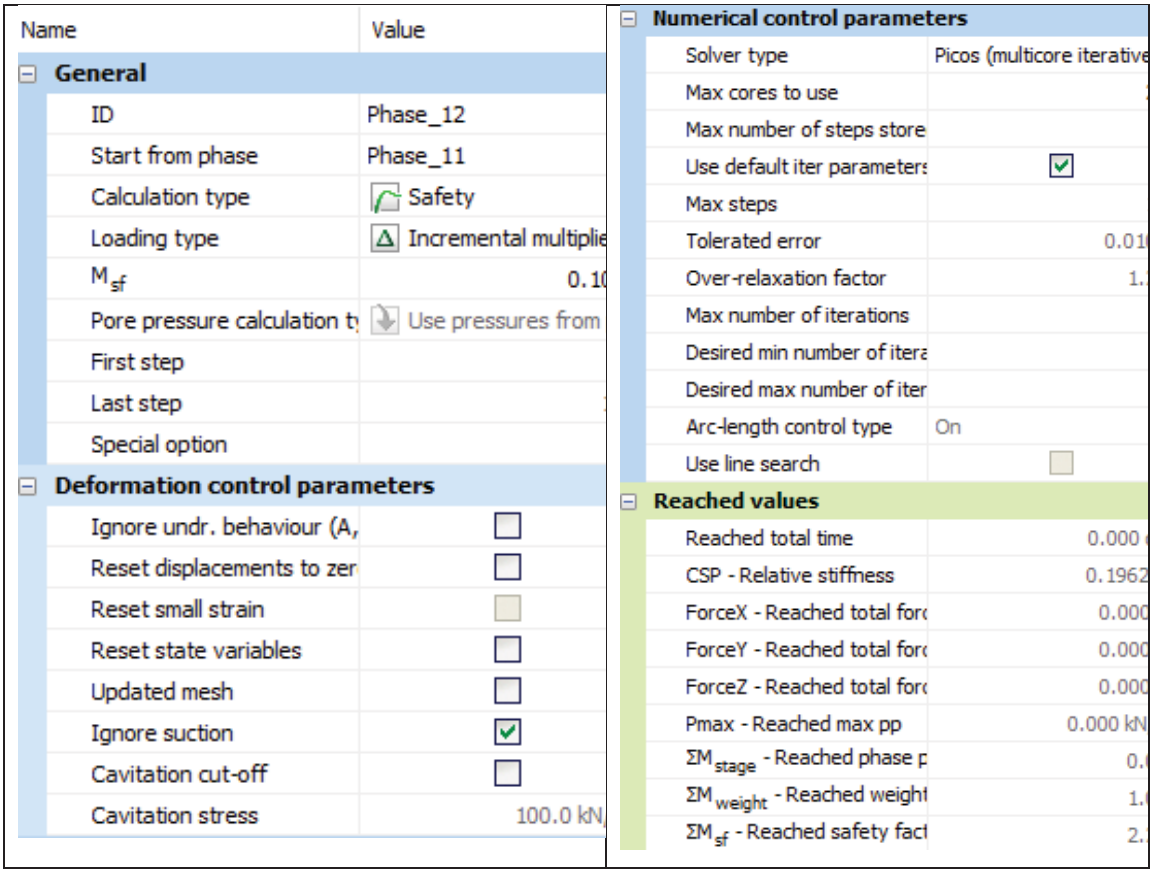

Figure 0-6: Safety Calculation Parameters

APPENDIX B – Plaxis Output

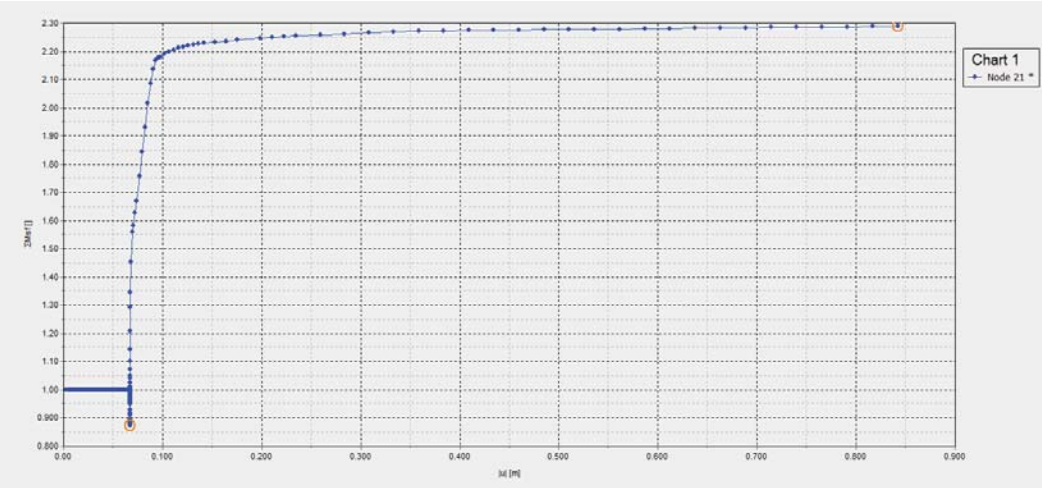

Figure 0-1 20kT FOS v total displacement

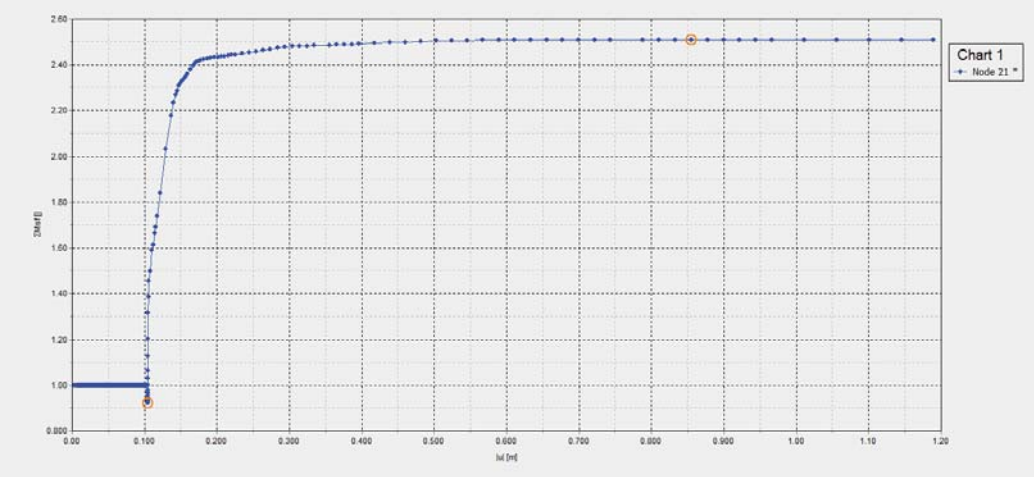

Figure 0-2: 30 kT FoS vs total displacement

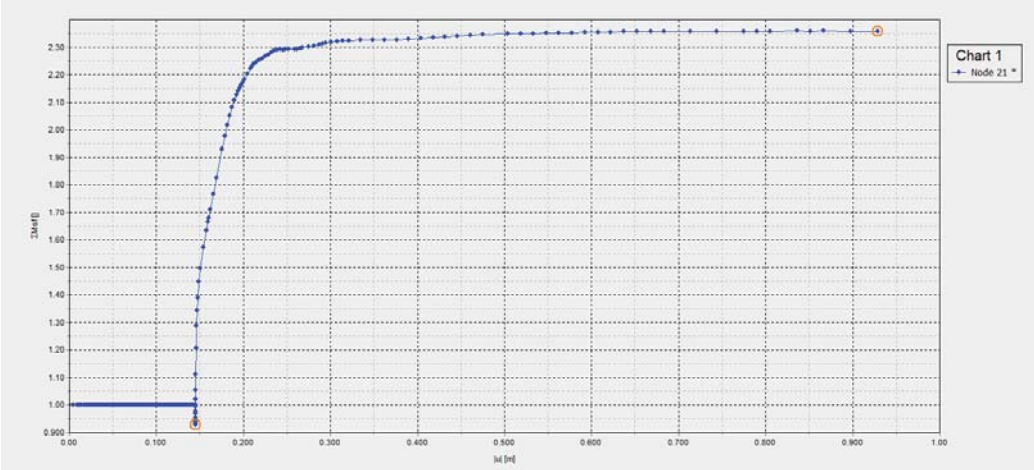

Figure 0-3: 40kt -FoS vs total displacement

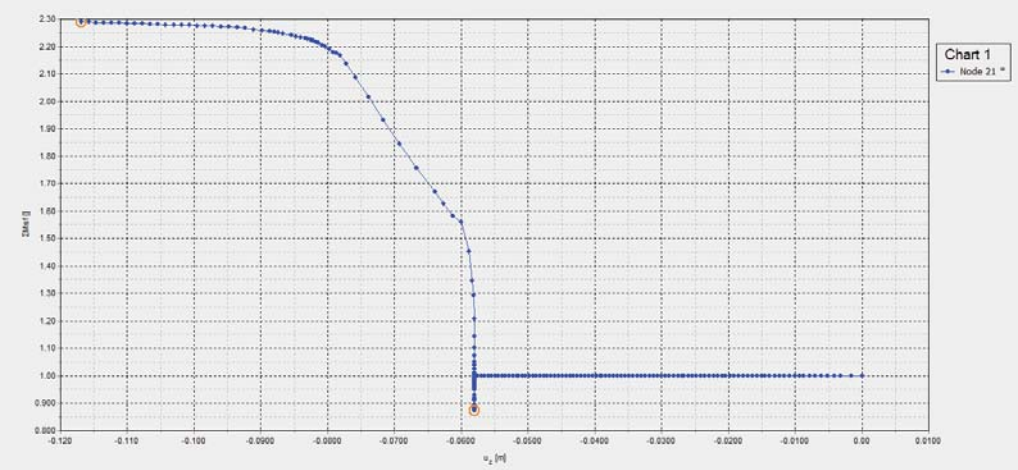

Figure 0-4: 20- kT vertical displacement vs FoS

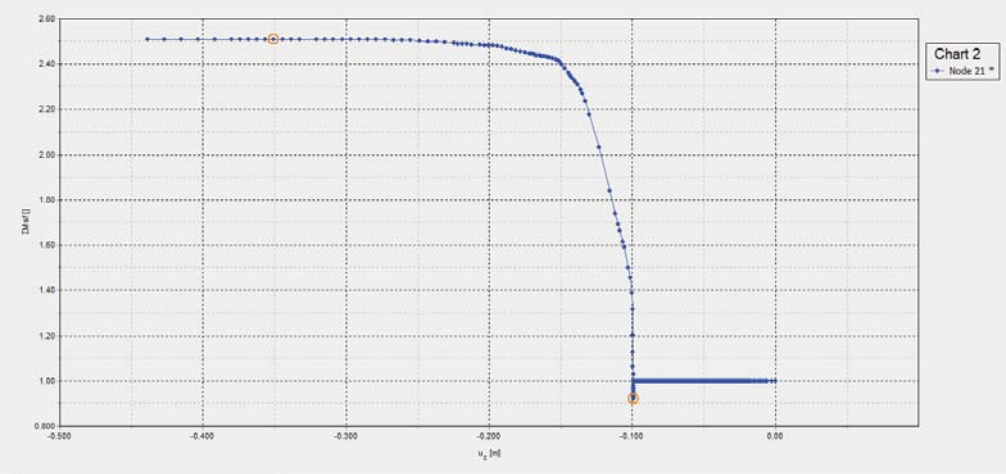

Figure 0-5: 30kT - Vertical displacement vs FoS

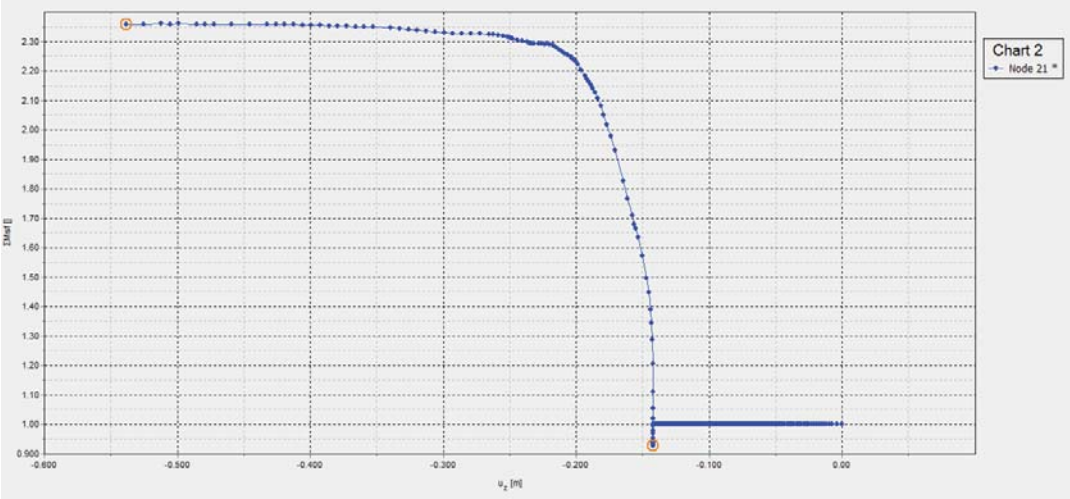

Figure 0-6: 40kT - Vertical displacement vs FoS

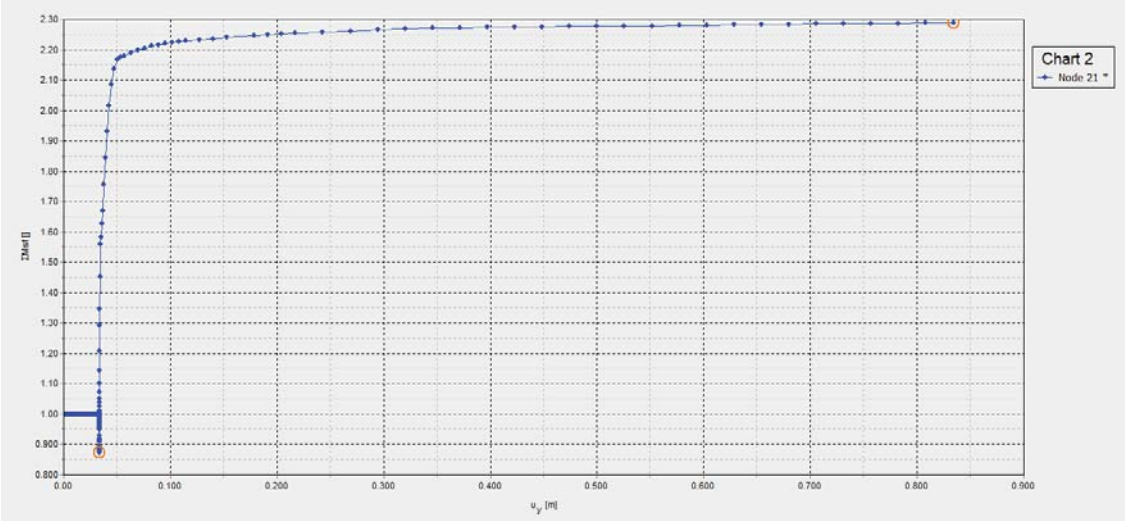

Figure 0-7: 20kT – Lateral displacement vs FoS

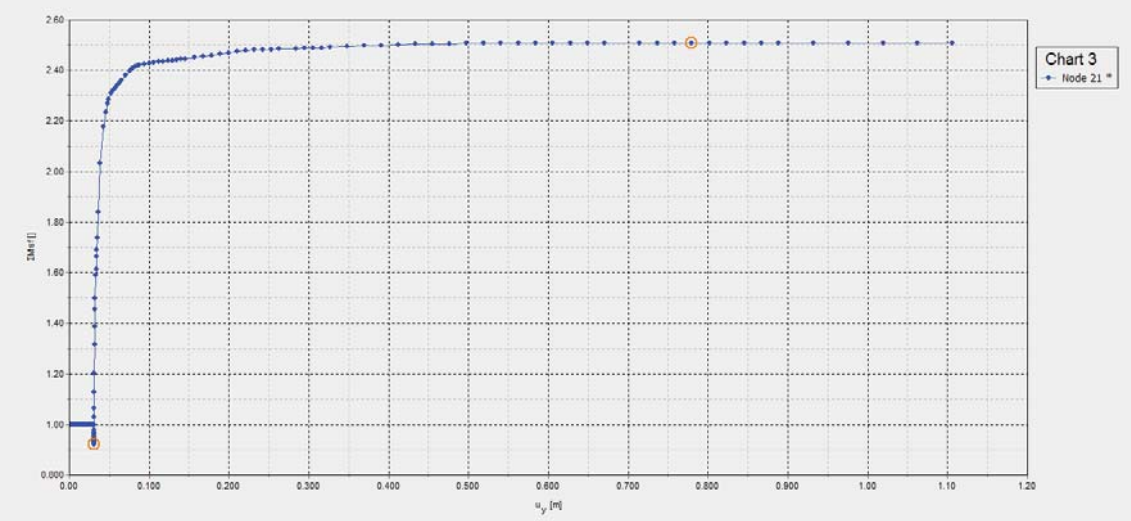

Figure 0-8. 30kT - Lateral displacement vs FoS

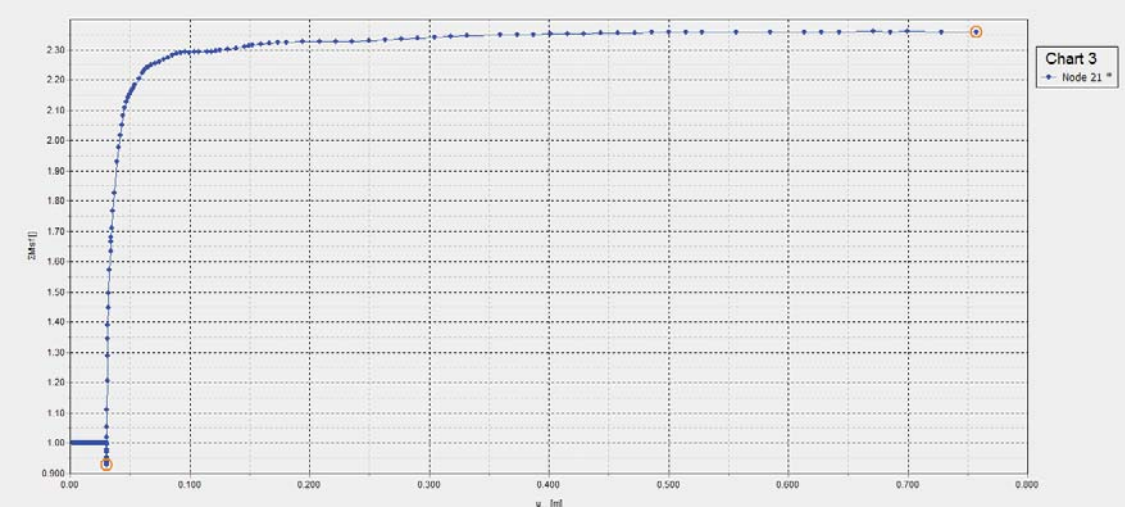

Figure 0-9: 40kT - Lateral displacement vs FoS